This article has been accepted for publication in a future issue of this journal, but has not been fully edited. Content may change prior to final publication. Citation information: DOI 10.1109/TAES.2017.2668078, IEEE Transactions on Aerospace and Electronic Systems

Navigation and control based on integral-uncertainty observer for unmanned jet aircraft

Xinhua Wang[1], Lilong Cai[2]

[1]Department of Electrical and Electronic Engineering, University of Nottingham, University Park, Nottingham, NG7 2RD, UK (Email: wangxinhua04@gmail.com)

[2]Department of Mechanical and Aerospace Engineering, Hong Kong University of Science and Technology, Hong Kong, China (Email: melcai@ust.hk)

Abstract: A nonlinear integral-uncertainty observer is presented, which can estimate the integral of measurement output signal and the uncertainty in system, synchronously. In order to be satisfied with the existing hardware computational environments and to select the parameters more easily, a simplified linear version of the nonlinear integral-uncertainty observer is also developed. The effectiveness of the proposed observers are verified through the numerical simulations and experiments: i) through the integral-uncertainty observers, the attitude angle and the uncertainties in attitude dynamics are estimated synchronously from the measurements of angular velocity, and the estimate results by the two observers are compared; ii) a control law is designed based on the observers to drive the jet aircraft to track a reference trajectory.

Keywords: Integral-uncertainty observer, jet aircraft, attitude angle, uncertainty, synchronous estimate

I. Introduction

Unmanned jet aircraft control has been an active area of investigation for several years, and some inertial sensors were used and supplemented by GPS [1, 2, 3]. This interest was motivated by the enormous military and civil applications of such aircraft. It is one of the most interesting architecture because its dynamical system is characterized by the powerful thrust provision, high-speed flight, the payload augmentation and a high maneuverability.

Usually, controlling an unmanned jet aircraft needs the information of the attitude and position. For the system of an unmanned jet aircraft, we consider that no measurement of flying velocity and attitude angle is provided. Moreover, jet aircrafts are underactuated mechanical systems, which exhibit high nonlinear, time-varying and time-delay behaviors, meanwhile, the influences of aerodynamic disturbance, unmodelled dynamics and parametric uncertainties are not avoidable in modeling. These nonlinearities and uncertainties render great challenges in the design of flight control system.

On the one hand, an inertial measurement unit (IMU) can provides the attitude information. It contains three orthogonal rate-gyroscopes and three orthogonal accelerometers, measuring angular velocity and linear acceleration, respectively. The information at high sampling frequency is provided by this sensor. To calculate the attitude angles of the device, the angular velocity signals from the rate-gyroscopes are onefold integrated. The drift phenomenon of IMU is mainly brought out by the usual integral methods [4, 5, 6, 7]: Romberg integration, Gaussian quadrature, extended Simpson's rule, low-frequency integrator. They cannot restrain the effect of stochastic noise (especially non-white noise). Such noise leads to the accumulation of additional drift in the integrated signal. In [8], a fractional-order integrator is proposed to approximate the irrational fractional-order integrator $1/s^m$. However, the condition of $0 < m < 1$ limits the application of the fractional-order integrator. Obviously, the usual observers or differentiators [9, 10, 11, 12] only can estimate the derivatives of the signal. Recent years, Kalman filter is used to handle the separation of probabilistic noise and to estimate signal integral [13, 14]. However, for Kalman filter, the process noise covariance and measurement noise covariance are assumed to be zero-mean Gaussian distributed, and the process noise covariance is uncorrelated to the estimation error. These assumptions are different from the real noise in signal. The inaccurate noise information in sensed angular velocity may lead to the estimate drifts of attitude angle. In [15], a nonlinear double-integral observer with the abilities of noise rejection and drift correction was presented to estimate synchronously the onefold and double integrals of a signal. In [16], a generalized multiple integrator was designed to estimate the multiple integrals for a signal. In [17], a nonlinear integral-derivative observer was proposed to estimate synchronously the integral and derivative of a signal. However, these observer cannot be use to estimate the uncertainties in the flight dynamics directly.

On the other hand, some sensors provide usually the position-related information. Representative designs are: GPS positioning systems [18, 19]; GPS/INS systems [20, 21, 22]; ultrasonic rangers [23]; GPS module when outdoors and infrared rangers when indoors [24]; carrier phase differential GPS [25]; laser rangefinder [26]; vision system [27, 28, 29]; indoor motion capture system [30, 31]; laser rangefinder and vision system [32]. However, these strategies are dependent on the accurate model, and all the states are required to be known.

For the aircrafts with uncertainties, sliding-mode controls with intelligent estimate algorithms were proposed [33, 34]. The uncertainties in aircraft are approximated by some intelligent algorithms, such as radial-based-function (RBF) networks or fuzzy systems. It was concluded that RBF networks are capable of universal approximation [35], and fuzzy system can also provide universal approximation for a continuous function [36]. However, the uncertainty estimation of aircraft by neural network or fuzzy system requires that all the states are known. The main difficulties with estimating uncertainties by these algorithms are: 1) the parameters or the neural network weights are difficult to be regulated; 2) membership function and Gaussian function are selected by experiences; 3) all of the system states must be required for estimation; 4) high-frequency noise cannot be restrained. These disadvantages affect control performances of aircraft adversely.

Considering the problems above, the objective of this paper is to design an observer to estimate the unknown integral state of measurement output signal and the uncertainty in system, synchronously, in spite of the existence of measurement disturbance. Inspired by the theory of finite-time stability [37,38], singular perturbation technique [39,40] and our previous works [15, 16], a nonlinear integral-uncertainty observer is developed. Based on the theories in [15, 16],

This article has been accepted for publication in a future issue of this journal, but has not been fully edited. Content may change prior to final publication. Citation information: DOI 10.1109/TAES.2017.2668078, IEEE Transactions on Aerospace and Electronic Systems

an extended system is implemented after the uncertainty in system is taken as a new state.

Thus, a nonlinear integral-uncertainty observer is developed, which can estimate the unknown integral state of measurement output signal and the uncertainty in system, synchronously. The parameters selection is satisfied with Routh-Hurwitz Stability Criterion and the iterative equation relations. Furthermore, considering of the adverse effects on the nonlinear system by the existing hardware computational environments in aircraft system, it is necessary to simplify the relatively complex nonlinear integral-uncertainty observer into a simple linear form, and the parameters selection needs to be more easier for some industrial applications. Fortunately, when some parameters in the nonlinear integral-uncertainty observer are given a particular value, the linear observer can be obtained, and it can still work. Although the nonlinear stability analysis no longer holds for the linear observer, the theory of linear system can be used to analyze it. The selection of parameters become relaxed, and it is only required to be satisfied with Routh-Hurwitz Stability Criterion. The parameters selection rules and robustness analysis for the two types of observers are presented based on frequency-domain analysis.

For industrial applications, the proposed observers are applied to an unmanned jet aircraft, and an experiment is presented to observe the performances of the proposed observers. In the jet aircraft system, the proposed observation algorithms are adopted to estimate the attitude angle and uncertainties in the attitude dynamics from the measurement of angular velocity, and the estimate results of the two integral-uncertainty observers are compared in the hardware computational environment. For the position dynamics, our previous designed augmented observer [41] is adopted to estimate the flying velocity and uncertainties from the GPS receiver signals. Finally, two controllers based on the observers are designed to stabilize the flight dynamics.

II. Design of integral-uncertainty observers

The following underactuated system has a minimum number of states and inputs but retains many of the features that must be considered when designing control laws for many mechanical systems:

$$\begin{aligned} \dot{w}_1 &= w_2 \\ \dot{w}_2 &= \Pi(t) + \sigma(t) \\ y_{op} &= w_2 + d(t) \end{aligned} \tag{1}$$

where, (w_1, w_2) is the state vector; $y_{op} = w_2 + d(t)$ is the measurement output; $d(t)$ is the bounded sensor error or stochastic noise, and $\sup_{t\in[0,\infty)} |d(t)| \le L_d < \infty$; w_1 is the unknown state; $\Pi(t) \in R$ is the known function; uncertainty $\sigma(t) \in R$ includes the unknown parameters and nonlinearities, and it is relatively bounded.

In order to calculate the unknown state w_1, the measurement signal y_{op} is integrated, i.e.,

$$I(t) = \int_0^t y_{op}(\sigma)\, d\sigma = \int_0^t w_2(\sigma)\, d\sigma + \int_0^t d(\sigma)\, d\sigma \tag{2}$$

Owing to the integration of Eq. (2), a small noise $d(t)$ (especially non-zero mean noise) in the measurement will grow rapidly in the computed final integration, i.e., the noise will be accumulated and accuracy in the computed final integration deteriorate with time. The error in the measurement signal is propagated to the integration. This results in integral drift. Moreover, the uncertainty $\sigma(t)$ renders great challenges in the design of control systems.

Assumption 1: Suppose the frequency of the uncertainty $\sigma(t)$ are far smaller than the system sampling frequency, and it has the following dynamics:

$$\dot{\sigma}(t) = c_\sigma(t) \tag{3}$$

In fact, this assumption is satisfied with almost all engineering applications, for instance, the dynamics of crosswind or the uncertainties in the aircraft systems.

Let $w_3 = \sigma(t)$, and $\dot{w}_3 = \dot{\sigma}(t) = c_\sigma(t)$, Eq. (1) can be augmented to

$$\begin{aligned} \dot{w}_1 &= w_2 \\ \dot{w}_2 &= w_3 + \Pi(t) \\ \dot{w}_3 &= c_\sigma(t) \\ y_{op} &= w_2 + d(t) \end{aligned} \tag{4}$$

2.1 Design of nonlinear integral-uncertainty observer

In the following, considering sensor error and noise, finite-time stability and robustness [37,38] (The related concepts are introduced in Appendix A) and singular perturbation technique [39,40] will be used to present an integral-uncertainty observer with drift correction and strong robustness. The onefold integral of measurement output signal and the uncertainty in system can be estimated, and the effect of propagating the noise to the integral is rejected sufficiently.

Theorem 1: For system (4), if the following observer is designed,

$$\begin{aligned} \dot{x}_1 &= x_2 \\ \dot{x}_2 &= x_3 + \Pi(t) \\ \varepsilon^4 \dot{x}_3 &= -k_1 |\varepsilon x_1|^{\alpha_1} sign(x_1) \\ &\quad -k_2 |x_2 - y_{op}|^{\alpha_2} sign(x_2 - y_{op}) \\ &\quad -k_3 \left|\varepsilon^3 x_3\right|^{\alpha_3} sign(x_3) \end{aligned} \tag{5}$$

where $\varepsilon \in (0,1)$ is the perturbation parameter, α_1, α_2 and α_3 satisfy:

$$\alpha_3 \in (0,1), \alpha_2 = \frac{\alpha_3}{2-\alpha_3}, \alpha_1 = \frac{\alpha_3}{3-2\alpha_3} \tag{6}$$

and $k_1, k_2, k_3 > 0$ are selected such that

$$k_1 > 0, k_3 > 0, k_2 > \varepsilon^{2\alpha_2} k_1 / k_3 \tag{7}$$

then there exist $\gamma > 1$, $L > 0$, $\delta_{di} \in (0,1)$ and $\Gamma > 0$, such that, for $t \ge \varepsilon\Gamma(\Xi(\varepsilon)e(0))$,

$$|x_i - w_i(t)| \le L(\delta_{di})^\gamma, i = 1,2,3 \tag{8}$$

This article has been accepted for publication in a future issue of this journal, but has not been fully edited. Content may change prior to final publication. Citation information: DOI 10.1109/TAES.2017.2668078, IEEE Transactions on Aerospace and Electronic Systems

Ideally, if no sensor error and noise exist, i.e., $d(t) = 0$ and $L_d = 0$, then, for $t \geq \varepsilon\Gamma\left(\Xi(\varepsilon)e\left(0\right)\right)$,

$$|x_i - w_i\left(t\right)| \leq L\varepsilon^{\alpha_1\gamma - i}, i = 1, 2, 3 \tag{9}$$

where $e_i = x_i - w_i\left(t\right)$, $i = 1, 2, 3$; $e = [\ e_1 \quad e_2 \quad e_3\ ]^T$; $\Xi(\varepsilon) = diag\{\varepsilon, \varepsilon^2, \varepsilon^3\}$.

The proof of Theorem 1 is presented in Appendix B.

In integral-uncertainty observer (5), x_2 tracks the state w_2; x_1 and x_3 estimate w_1 and the uncertainty w_3 (i.e., $\sigma(t)$ in system (1)), respectively. The usual integral algorithms inevitably suffer from unbounded errors in the calculations of integral when noise exists in measurement output signal y_{op}. However, from (8), the up-boundness of the estimate errors are bounded, and they are unrelated to integration time.

In fact, in the up-boundness of estimate error $L(\delta_{di})^\gamma$ $(i = 1, 2, 3)$, $\gamma > 1$ holds, and from the proof of Theorem 1 in Appendix B, $L = \mu\delta_0^\gamma$, where μ is a constant defined in Theorem 5.2 in [37]. For the low-level noise, from (88), $\delta_{di} \in (0, 1)$ holds. By selecting a suitable perturbation parameter $\varepsilon \in (0, 1)$, the up-boundness of estimate errors are sufficiently small. Therefore, the ultimate bound (8) on the estimation error is of higher order than the perturbation. Consequently, the presented double-integral observer (5) leads to perform rejection of low-level noise, i.e., almost no drift phenomenon happen in spit of the existence of the sensor error and non-white noise.

2.2 Design of linear integral-uncertainty observer

As we know, a linear system is easy to perform the analysis with respect to nonlinear one. In the following, based on the nonlinear integral-uncertainty observer (5), a simplified linear integral-uncertainty observer will be designed, and Theorem 2 is presented as follow.

Corollary 1: For system (4), if the following observer is designed,

$$\begin{aligned} \dot{x}_1 &= x_2 \\ \dot{x}_2 &= x_3 + \Pi(t) \\ \varepsilon^4\dot{x}_3 &= -k_1\varepsilon x_1 - k_2\left(x_2 - w_2\right) - k_3\varepsilon^3 x_3 \end{aligned} \tag{10}$$

where $\varepsilon \in (0, 1)$ is the perturbation parameter, and

$$k_1 > 0, k_3 > 0, k_2 > \varepsilon^2 k_1/k_3 \tag{11}$$

then the following estimate relations hold:

$$\lim_{\varepsilon\to 0} x_i = w_i \tag{12}$$

where $i = 1, 2, 3$. The relevant analysis of Corollary 1 is presented in Appendix B.

In integral-uncertainty observer (10), x_2 tracks the state w_2; x_1 and x_3 estimate w_1 and the uncertainty w_3 (i.e., $\sigma(t)$ in system (1)), respectively. The proposed two observers (5) and (10) all can perform rejection of high-frequency noise. In the next section, the frequency-domain analysis will be presented for the nonlinear and linear observers, and the parameters selection rules will be given.

III. ROBUSTNESS ANALYSIS AND PARAMETERS SELECTION

In practice, high-frequency noises exist in measurement output y_{op}. In this paper, describing function method [40, 42] is used to approximately analyze and predict the nonlinear behaviors of the observer. Even though it is only an approximation method, the desirable properties it inherits from the frequency response method, and the shortage of other, systematic tools for nonlinear observer analysis, make it an indispensable component of the bag of tools of practicing control engineers. The describing function method succeeded in applications to analyze the frequency-domain characteristics for nonlinear differentiators and augmented observers [41]. By describing function method, it will be found that the presented integral-uncertainty observer leads to perform rejection of high-frequency noise. Alternatively, the frequency-sweep method [43, 44] can be used to approximately analyze and predict the nonlinear behaviors of these observers.

In addition, there exist seven parameters in nonlinear observer (5): α_1, α_2, α_3, k_1, k_3, k_1, ε; and four parameters in linear observer (10): k_1, k_3, k_1, ε. How to select these parameters is critical for the estimate performances and robustness abilities.

For system (4), let $\xi_1 = w_1$, $\xi_2 = w_2$, $\xi_3 = w_3 + \Pi(t)$ and $\dot{\Pi}(t) = \eta(t)$, then $\dot{w}_3 + \dot{\Pi}(t) = c_\sigma(t) + \eta(t)$. Therefore, system (4) can be rewritten as

$$\begin{aligned} \dot{\xi}_1 &= \xi_2 \\ \dot{\xi}_2 &= \xi_3 \\ \dot{\xi}_3 &= c_\sigma(t) + \eta(t) \\ y_{op} &= \xi_2 \end{aligned} \tag{13}$$

Accordingly, for system (13), the observer (5) can be transferred to

$$\begin{aligned} \dot{x}_1 &= x_2 \\ \dot{x}_2 &= x_3 \\ \varepsilon^4\dot{x}_3 &= -k_1\left|\varepsilon x_1\right|^{\alpha_1} sign\left(x_1\right) \\ &\quad -k_2\left|x_2 - y_{op}\right|^{\alpha_2} sign\left(x_2 - y_{op}\right) \\ &\quad -k_3\left|\varepsilon^3 x_3\right|^{\alpha_3} sign\left(x_3\right) \end{aligned} \tag{14}$$

where x_2 tracks the output signal ξ_2; x_1 and x_3 estimate ξ_1 and ξ_3, respectively.

The frequency characteristic of (14) is analyzed as follow.

Let $x_2 - y_{op} = A\sin(\omega t)$. For the nonlinear function $|A\sin(\omega t)|^{\alpha_i} sign(\sin(\omega t))$, its describing functions can be obtained as follow:

$$\begin{aligned} N_i(A) &= \frac{2}{A\pi}\int_0^\pi |A\sin(\omega\tau)|^{\alpha_i} sign(A\sin(\omega\tau))\sin(\omega\tau)d\omega\tau \\ &= \frac{\Omega(\alpha_i)}{A^{1-\alpha_i}} \end{aligned}$$

where $\Omega(\alpha_i) = \frac{2}{\pi}\int_0^\pi |\sin(\omega\tau)|^{\alpha_i+1} d\omega\tau$. Therefore, the linearization of observer (14) is

This article has been accepted for publication in a future issue of this journal, but has not been fully edited. Content may change prior to final publication. Citation information: DOI 10.1109/TAES.2017.2668078, IEEE Transactions on Aerospace and Electronic Systems

$$\begin{aligned}\dot{x}_1 &= x_2\\ \dot{x}_2 &= x_3\\ \varepsilon^4\dot{x}_3 &= -k_1\frac{\Omega(\alpha_1)}{A^{1-\alpha_1}}\varepsilon x_1 - k_2\frac{\Omega(\alpha_2)}{A^{1-\alpha_2}}(x_2-y_{op})\\ &\quad -k_3\frac{\Omega(\alpha_3)}{A^{1-\alpha_3}}\varepsilon^3 x_3\end{aligned} \tag{15}$$

and the Laplace transformations of the linear system (15) can be written as

$$\begin{aligned}sX_1(s) &= X_2(s)\\ sX_2(s) &= X_3(s)\\ \varepsilon^4 sX_3(s) &= -k_1\frac{\Omega(\alpha_1)}{A^{1-\alpha_1}}\varepsilon X_1(s)\\ &\quad -k_2\frac{\Omega(\alpha_2)}{A^{1-\alpha_2}}(X_2(s)-Y_{op}(s))\\ &\quad -k_3\frac{\Omega(\alpha_3)}{A^{1-\alpha_3}}\varepsilon^3 X_3(s)\end{aligned} \tag{16}$$

where $X_i(s)$ and $Y_{op}(s)$ denote the Laplace transformations of x_i and y_{op}, respectively, and s denotes Laplace operator.

From Eq. (16), the following transfer functions are obtained:

$$\begin{aligned}\frac{X_j(s)}{Y_{op}(s)} &= \frac{k_2\frac{\Omega(\alpha_2)}{A^{1-\alpha_2}}s^{j-1}}{\varepsilon^4 s^3+\varepsilon^3 k_3\frac{\Omega(\alpha_3)}{A^{1-\alpha_3}}s^2+k_2\frac{\Omega(\alpha_2)}{A^{1-\alpha_2}}s+\varepsilon k_1\frac{\Omega(\alpha_1)}{A^{1-\alpha_1}}}\\ j &\in \{1,2,3\}\end{aligned} \tag{17}$$

The transfer functions for linear observer (10) can be directly obtained as

$$\frac{X_j(s)}{Y_{op}(s)} = \frac{k_2 s^{j-1}}{\varepsilon^4 s^3+\varepsilon^3 k_3 s^2+k_2 s+\varepsilon k_1}, j\in\{1,2,3\} \tag{18}$$

The effects of the observer parameters on the robustness are analyzed as follows.

3.1 Frequency characteristic with different ε and α_3

Selecting α_3 with different values, we obtain the following table of $\Omega(\alpha_3)$, $\Omega(\alpha_2)$ and $\Omega_3(\alpha_1)$:

α_3	$\Omega(\alpha_3)$	$\Omega(\alpha_2)$	$\Omega(\alpha_1)$
0.8	1.0410	1.0712	1.0944
0.5	1.1128	1.1596	1.1852
0.3	1.1697	1.2093	1.2270

Table 1 Values of $\Omega(\alpha_3)$, $\Omega(\alpha_2)$ and $\Omega(\alpha_1)$ with respect to α_3

For the transfer functions (17) and (18), the parameters are selected as follows: $k_1=0.1$, $k_2=2$, $k_3=1$; $A=1$; $\alpha_3=0.3,0.5,1$, respectively; $R=1/\varepsilon=3,4,5$, respectively. The Bode plots of the frequency-domain characteristics with different ε and α_3 are described in Figs.1(a), 1(b) and 1(c), respectively: Fig.1(a) presents the frequency characteristics of the transfer functions of signal tracking; Figs.1(b) and 1(c) present the frequency characteristics of the transfer functions of integral and derivative estimations, respectively.

Particularly, in comparing with ideal integral operators $1/s$ and s, not only the observers can obtain their estimations precisely, but also the high-frequency noise is rejected sufficiently.

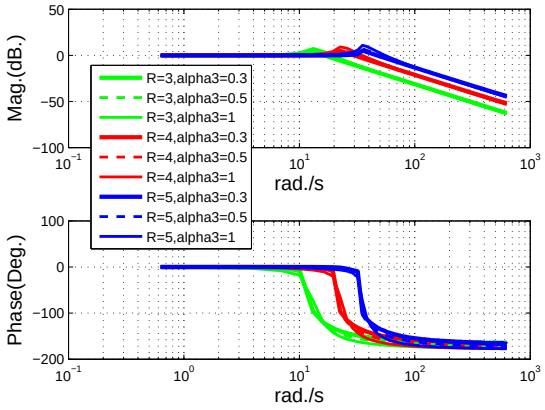

(a)

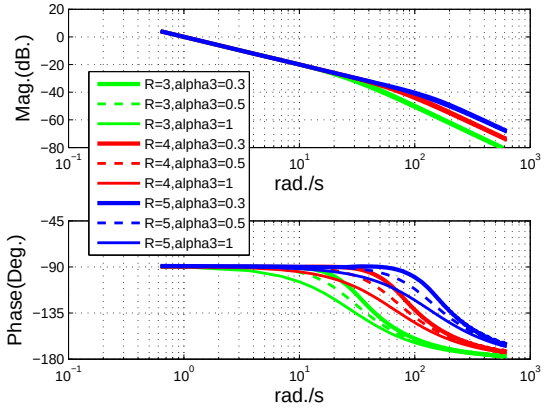

(b)

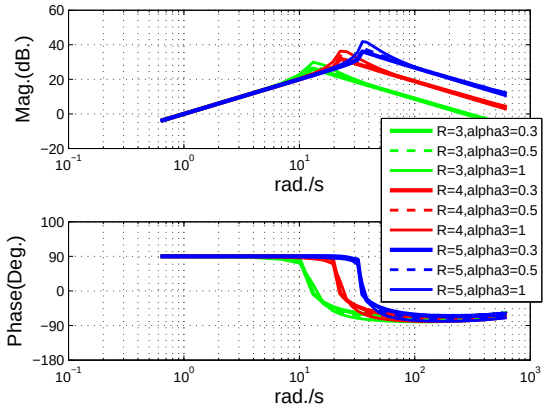

(c)

Fig. 1. Frequency characteristics with the change of ε and α for integral-uncertainty observers. (a) Transfer function $X_2(s)/Y_{op}(s)$. (b) Transfer function $X_1(s)/Y_{op}(s)$. (c) Transfer function $X_3(s)/Y_{op}(s)$.

This article has been accepted for publication in a future issue of this journal, but has not been fully edited. Content may change prior to final publication. Citation information: DOI 10.1109/TAES.2017.2668078, IEEE Transactions on Aerospace and Electronic Systems

Parameter ε affects the low-pass frequency bandwidth: Decreasing the perturbation parameter ε, the low-pass frequency bandwidth is larger, the estimation precision becomes better, and relatively higher frequency noise can be reduced; on the other hand, increasing perturbation parameter ε, the low-pass frequency bandwidth is smaller, much noise can be reduced sufficiently (See the cases of $R = 1/\varepsilon = 3, 4, 5$ in Fig.1, respectively). Parameter $\alpha_3 \in (0, 1]$ affects the decay speed of frequency characteristic curves near the cut-off frequency (See the cases of $\alpha_3 = 0.3, 0.5, 1$ in Fig.1, respectively): Smaller $\alpha_3 \in (0, 1]$ can obtain more precise estimations; Larger $\alpha_3 \in (0, 1]$ can reduce much noise, however, a bit estimation delay happens.

3.2 The proposed rules of parameters selection

For nonlinear integral-uncertainty observer (5), there are some rules suggested on the parameters selection:

1) The parameters $\alpha_1, \alpha_2, \alpha_3, k_1, k_2$ and k_3 are satisfied with the conditions (6) and (7).

2) When the up-boundness of the integral, the uncertainty $\sigma(t)$ or the derivative $c_\sigma(t)$ of signal $\sigma(t)$ increase, i.e., h_1, h_3 or L_a increase, δ_0 in (80) will increase, and $L = \mu\delta_0^\gamma$ also increases, where μ is a constant defined in Theorem 5.2 in [37]. Perturbation parameter $\varepsilon \in (0, 1)$ should decrease to improve the estimation precisions.

3) When the magnitude of the noise increases, i.e., L_d increases, in order to decrease $L_d^{\alpha_2}$ in (80), $\alpha_2 \in (0, 1)$ should increase to improve the estimate precisions. In fact, for $L_d \in (0, 1)$ and $\alpha_{21}, \alpha_{22} \in (0, 1)$, if $\alpha_{22} > \alpha_{21}$, then $L_d^{\alpha_{22}} < L_d^{\alpha_{21}}$ holds.

The parameters selection of linear observer (10) is easier than that of nonlinear observer (5): Parameters k_1, k_2 and k_3 decide the observer stability, and they should be satisfied with the conditions (11). The selection of ε decides the estimate precision and robustness: when the up-boundness of the integral, the uncertainty $\sigma(t)$ or the derivative $c_\sigma(t)$ of signal $\sigma(t)$ increase, i.e., h_1, h_3 or L_a increase, $\varepsilon \in (0, 1)$ should decrease to improve the estimation precisions; if much noise exists, ε should increase, the low-pass frequency bandwidth is smaller, much noise can be reduced sufficiently.

To evaluate the theory of the proposed integral-uncertainty observers, they will be applied to an unmanned jet aircraft.

IV. Application to an Unmanned Jet Aircraft

4.1 Modeling of jet aircraft

The proposed observers are applied to control an unmanned jet aircraft, which is shown in Fig.2, and the forces and torques of the aircraft are denoted in Fig.3.

1) Coordinates and frames

Let $\Xi_g = (E_x, E_y, E_z)$ denote the right handed inertial frame and $\Xi_b = \left(E_x^b, E_y^b, E_z^b\right)$ denote the frame attached to the aircraft's fuselage whose origin is located at its center of gravity. $\Theta = (\psi, \theta, \phi)$ describes the aircraft orientation expressed in the classical yaw, pitch and roll angles. We use c_θ for $\cos\theta$ and s_θ for $\sin\theta$. R is the transformation matrix representing the orientation of the aircraft from frame Ξ_b to Ξ_g, i.e.,

Fig. 2. An unmanned jet aircraft.

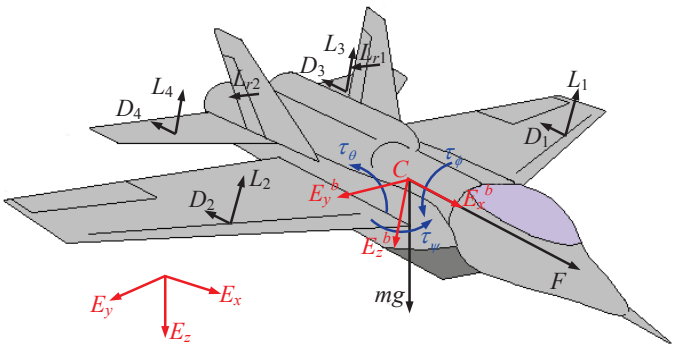

Fig. 3. Forces and torques illustration of the unmanned jet aircraft.

$$R = \begin{bmatrix} c_\theta c_\psi & c_\psi s_\theta s_\phi - s_\psi c_\phi & c_\psi s_\theta c_\phi + s_\psi s_\phi \\ c_\theta s_\psi & s_\psi s_\theta s_\phi + c_\psi c_\phi & s_\psi s_\theta c_\phi - c_\psi s_\phi \\ -s_\theta & s_\phi c_\theta & c_\phi c_\theta \end{bmatrix} \tag{19}$$

Let α and β be the angle of attack of the fixed wing and the sideslip angle, respectively, thus

$$\alpha = \theta - \arctan^{-1}(\dot{z}_s/\dot{x}_s), \beta = \arcsin^{-1}(\dot{y}_s/v_s) \tag{20}$$

where, and the relative wind speed $(\dot{x}_s, \dot{y}_s, \dot{z}_s)$ is measured by the airspeed tube, and $v_s = \sqrt{\dot{x}_s^2 + \dot{y}_s^2 + \dot{z}_s^2}$.

Define (x, y, z) and $(\dot{x}, \dot{y}, \dot{z})$ as the position of center of gravity and the velocity to frame Ξ_g, body force $F \in \Re^3$ and torque $\tau \in \Re^3$.

The total external force F consists of the thrust F_c generated by the jet engine, aerodynamic forces on the fixed wing F_w, aerodynamic forces on the fuselage F_f, the forces created by the verticals F_v, the forces created by the elevators F_e, and uncertainties and external disturbances F_d. These forces are expressed in body frame Ξ_b, and they are transformed by R to be expressed in the inertial frame Ξ_g as follows:

$$F = R(F_c + F_w + F_f + F_v + F_e + F_d) \tag{21}$$

The total moment τ consists of the moments created by the fixed wings τ_w, the moments created by the verticals τ_v, the moments created by the elevators τ_e, and moments due to the uncertainties and external disturbances τ_d:

$$\tau = \tau_w + \tau_v + \tau_e + \tau_d \tag{22}$$

This article has been accepted for publication in a future issue of this journal, but has not been fully edited. Content may change prior to final publication. Citation information: DOI 10.1109/TAES.2017.2668078, IEEE Transactions on Aerospace and Electronic Systems

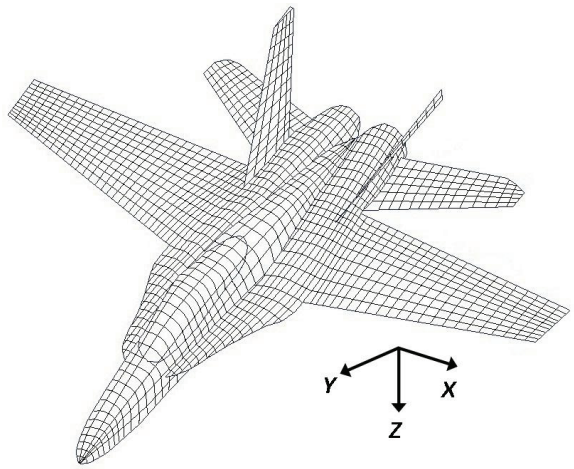

Fig. 4. Mesh of jet aircraft.

Fluent software is used to simulate the flying environment to obtain the parameters, and the results are compared to those from the wind tunnel tests. Fluent is one of the applications of computing fluid dynamics [45]. It uses finite-element method to calculate the motion of fluid field, and three steps are arranged to get the aerodynamic parameters [46]. The parameters of fixed wings, fuselage, elevator and vertical are obtained by using the 3-D simulation shown in Fig.4.

2) The aerodynamic parameters of fixed wings

The lift force and drag forces generated by the fixed wings are, respectively

$$\begin{aligned} L_i &= 0.5C_{Li}S\rho(\dot{x}_s^2+\dot{z}_s^2), C_{Li}=C_{L0}+C_{L\alpha}\alpha+C_{L\delta_i}\delta_i \\ D_i &= 0.5C_{Di}S\rho(\dot{x}_s^2+\dot{z}_s^2), C_{Di}=C_{D0}+C_{Li}^2/(\pi A_w e_w), \\ e_w &= 1.78(1-0.045A_w^{0.68})-0.46 \end{aligned} \quad (23)$$

where $i=1,2$; S is the area of the half wing, C_{L0} is the lift coefficient when the angle of attack α is equal to zero, $C_{L\alpha}$ is the lift coefficient due to the angle of attack α, δ_i is the normal flap bias angle, and $C_{L\delta_i}$ is the lift coefficient due to the flap bias angle δ_i. A_w is the aspect ratio of the fixed wing. e_w is the value of the Oswald's efficiency factor. The expression of lift and drag coefficients is considered as valid for low angles of attack.

Then the aerodynamic forces on the fixed wings F_w in body frame can be written as

$$F_w=\begin{bmatrix} (L_1+L_2)\sin\alpha-(D_1+D_2)\cos\alpha \\ 0 \\ -(L_1+L_2)\cos\alpha-(D_1+D_2)\sin\alpha \end{bmatrix} \quad (24)$$

and the moments created by the aerodynamic forces produced by the wings τ_w are

$$\tau_w=\begin{bmatrix} l_w[(L_1-L_2)\cos\alpha+(D_1-D_2)\sin\alpha] \\ l_c[(L_2+L_1)\cos\alpha+(D_2+D_1)\sin\alpha] \\ l_w[(L_1-L_2)\sin\alpha+(D_2-D_1)\cos\alpha] \end{bmatrix} \quad (25)$$

3) The aerodynamic parameters of fuselage

The parameters of fuselage lift and drag are presented as follows:

$$\begin{aligned} L_f &= 0.5\rho C_{lf}S_f(\dot{x}_s^2+\dot{z}_s^2), D_f=0.5\rho C_{df}S_f(\dot{x}_s^2+\dot{z}_s^2), \\ C_{lf} &= C_{lf\alpha}\alpha, C_{df}=C_{df0}+C_{df\alpha}\alpha \end{aligned} \quad (26)$$

where L_f and D_f are the lift and drag forces generated by the fuselage, respectively; C_{lf} is the lift coefficient; C_{df} is the drag coefficient; C_{df0} is the constant in the coefficient of drag force. Then the forces on the fuselage F_f in body frame are written as

$$F_f=\begin{bmatrix} L_f\sin\alpha-D_f\cos\alpha \\ 0 \\ -L_f\cos\alpha-D_f\sin\alpha \end{bmatrix} \quad (27)$$

4) The aerodynamic parameters of level stabilizer

The parameters of elevator lift and drag are presented as follows:

$$\begin{aligned} L_e &= 0.5C_{le}S_e\rho(\dot{x}_s^2+\dot{z}_s^2), C_{le}=C_{le\alpha}(\alpha+\delta_e) \\ D_e &= 0.5C_{de}S_e\rho(\dot{x}_s^2+\dot{z}_s^2), C_{de}=C_{de0}+C_{le}^2/(\pi A_e e_e), \\ e_e &= 1.78(1-0.045A_e^{0.68})-0.46 \end{aligned} \quad (28)$$

where S_e is the area of the level stabilizer, δ_e is the bias angle of elevator, and $C_{le\delta_e}$ is the lift coefficient due to the bias angle δ_e, $C_{le\alpha}$ is the lift coefficient due to the angle of attack α and the normal bias angle δ_e. A_e is the aspect ratio of the level stabilizer. e_e is the value of the Oswald's efficiency factor. Then the force F_e on the level stabilizer in body frame are written as

$$F_e=\begin{bmatrix} L_e\sin(\alpha+\delta_e)-D_e\cos(\alpha+\delta_e) \\ 0 \\ -L_e\cos(\alpha+\delta_e)-D_e\sin(\alpha+\delta_e) \end{bmatrix} \quad (29)$$

and the moment τ_e created by the aerodynamic forces produced by the level stabilizer is

$$\tau_e=\begin{bmatrix} 0 \\ -l_e[L_e\cos(\alpha+\delta_e)+D_e\sin(\alpha+\delta_e)] \\ 0 \end{bmatrix} \quad (30)$$

5) The aerodynamic parameters of vertical stabilizer

The lift force and drag forces generated by the vertical stabilizer, respectively

$$\begin{aligned} L_v &= 0.5C_{lv}S_v\rho(\dot{x}_s^2+\dot{z}_s^2), C_{lv}=C_{lv\beta}\beta+C_{lv\delta_v}\delta_v \\ D_v &= 0.5C_{dv}S_v\rho(\dot{x}_s^2+\dot{z}_s^2), C_{dv}=C_{dv0}+C_{lv}^2/(\pi A_v e_v), \\ e_v &= 1.78(1-0.045A_v^{0.68})-0.46 \end{aligned} \quad (31)$$

where S_v is the area of the half wing, $C_{lv\alpha}$ is the lift coefficient due to the angle of attack α, δ_v is the bias angle of rudder, and $C_{lv\delta_v}$ is the lift coefficient due to the bias angle δ_v. A_e is the aspect ratio of the fixed wing. e_v is the value of the Oswald's efficiency factor.

Then the aerodynamic force F_v on the vertical stabilizer in body frame can be written as

This article has been accepted for publication in a future issue of this journal, but has not been fully edited. Content may change prior to final publication. Citation information: DOI 10.1109/TAES.2017.2668078, IEEE Transactions on Aerospace and Electronic Systems

$$F_v = \begin{bmatrix} L_v \sin\beta - D_v \cos\beta \\ L_v \cos\beta + D_v \sin\beta \\ 0 \end{bmatrix} \quad (32)$$

and the moment τ_v created by the aerodynamic forces produced by the vertical stabilizer is

$$\tau_v = \begin{bmatrix} l_{v1}[L_v \cos\alpha + D_v \sin\alpha] \\ 0 \\ l_{v2}[L_v \cos\alpha + D_v \sin\alpha] \end{bmatrix} \quad (33)$$

6) Motion equation of the jet aircraft

The equations of motion written in terms of the centre of mass C in the fixed axes of coordinate (x, y, z) are then

$$\begin{aligned} m\ddot{x} &= c_\theta c_\psi F_c + F_{wx} + F_{fx} + F_{vx} + F_{ex} + \Delta_x \\ m\ddot{y} &= c_\theta s_\psi F_c + F_{wy} + F_{fy} + F_{vy} + F_{ey} + \Delta_y \\ m\ddot{z} &= -s_\theta F_c - mg + F_{wz} + F_{fz} + F_{vz} + F_{ez} \\ &\quad +\Delta_z \end{aligned} \quad (34)$$

$$\begin{aligned} J_z\ddot{\psi} &= \dot{\theta}\dot{\phi}(J_x - J_y) - k_\psi\dot{\psi} + \tau_\psi + \Delta_\psi \\ J_y\ddot{\theta} &= \dot{\psi}\dot{\phi}(J_z - J_x) - k_\theta\dot{\theta} + \tau_\theta + \Delta_\theta \\ J_x\ddot{\phi} &= \dot{\psi}\dot{\theta}(J_y - J_z) - k_\phi\dot{\phi} + \tau_\phi + \Delta_\phi \end{aligned} \quad (35)$$

where J_x, J_y and J_z are the three-axis moment of inertias; k_ψ, k_θ and k_ϕ are the drag coefficients; m is the mass of the aircraft; g is the gravity acceleration; Δ_x, Δ_y and Δ_z are the bounded disturbances or uncertainties in the position dynamics; Δ_ψ, Δ_θ and Δ_ϕ are the bounded disturbances or uncertainties in the attitude dynamics; τ_ψ, τ_θ and τ_ϕ are the control torques for yaw, pitch and roll dynamics, respectively, and they are selected as

$$\begin{aligned} \tau_\psi &= 0.5 l_{v2}(\dot{x}_s^2 + \dot{z}_s^2)\rho S_v C_{lv\delta_v}\delta_v \\ \tau_\theta &= -0.5 l_e(\dot{x}_s^2 + \dot{z}_s^2)\rho S_e C_{le\alpha}\delta_e \\ \tau_\phi &= l_w C_{L\delta_i} S\rho(\dot{x}_s^2 + \dot{z}_s^2)\delta_{1,2}, \end{aligned} \quad (36)$$

where $\delta_1 = -\delta_2 = \delta_{1,2}$, and

$$\begin{bmatrix} F_{wx} + F_{fx} + F_{vx} + F_{ex} \\ F_{wy} + F_{fy} + F_{vy} + F_{ey} \\ F_{wz} + F_{fz} + F_{vz} + F_{ez} \end{bmatrix} = R(F_w + F_f + F_v + F_e) \quad (37)$$

The tracking control problem for the jet aircraft can be stated mathematically as: For the reference trajectory (x_d, y_d, z_d) in the inertial frame, find the control laws such that the following statements hold:

i) $x \to x_d, \dot{x} \to \dot{x}_d, y \to y_d, \dot{y} \to \dot{y}_d, z \to z_d, \dot{z} \to \dot{z}_d$ as $t \to \infty$; ii) The whole closed-loop system is stable.

Here, we are interested in adopting the presented observers to estimate the attitude angle (ψ, θ, ϕ) and the uncertainties in the attitude dynamics from the measurement of the angular rate $(\dot{\psi}, \dot{\theta}, \dot{\phi})$ of IMU . Moreover, our previous augmented observer [41] will be used to estimate the velocity $(\dot{x}, \dot{y}, \dot{z})$ and the uncertainties in the position dynamics from the measurement of the position (x, y, z). Finally, the controller will be designed to implement the tracking control for the jet aircraft.

4.2 Design of integral-uncertainty observers for the jet aircraft

For Eqs. (34) and (35), it is considered that $(\dot{x}, \dot{y}, \dot{z})$ and (ψ, θ, ϕ) are not measured directly, $(k_x,\ k_y,\ k_z,\ k_\psi,\ k_\theta,\ k_\phi)$ and $(\Delta_x,\ \Delta_y,\ \Delta_z,\ \Delta_\psi,\ \Delta_\theta,\ \Delta_\phi)$ are bounded and unknown. Let $w_{1,1} = x$, $w_{1,2} = \dot{x}$, $w_{2,1} = y$, $w_{2,2} = \dot{y}$, $w_{3,1} = z$, $w_{3,2} = \dot{z}$, $w_{4,1} = \psi$, $w_{4,2} = \dot{\psi}$, $w_{5,1} = \theta$, $w_{5,2} = \dot{\theta}$, $w_{6,1} = \phi$, $w_{6,2} = \dot{\phi}$, and

$$\begin{aligned} \Pi_1(t) &= \frac{c_\theta c_\psi F_c + F_{wx} + F_{fx} + F_{vx} + F_{ex}}{m}, \\ \Pi_2(t) &= \frac{c_\theta s_\psi F_c + F_{wy} + F_{fy} + F_{vy} + F_{ey}}{m}, \\ \Pi_3(t) &= \frac{-s_\theta F_c - mg + F_{wz} + F_{fz} + F_{vz} + F_{ez}}{m}, \\ \sigma_1(t) &= \frac{\Delta_x}{m}, \sigma_2(t) = \frac{\Delta_y}{m}, \sigma_3(t) = \frac{\Delta_z}{m} \end{aligned} \quad (38)$$

$$\begin{aligned} \Pi_4(t) &= \frac{\dot{\theta}\dot{\phi}(J_x - J_y) + \tau_\psi}{J_z}, \Pi_5(t) = \frac{\dot{\psi}\dot{\phi}(J_z - J_x) + \tau_\theta}{J_y}, \\ \Pi_6(t) &= \frac{\dot{\psi}\dot{\theta}(J_y - J_z) + \tau_\phi}{J_x}, \sigma_4(t) = \frac{-k_\psi\dot{\psi} + \Delta_\psi}{J_z}, \\ \sigma_5(t) &= \frac{-k_\theta\dot{\theta} + \Delta_\theta}{J_y}, \sigma_6(t) = \frac{-k_\phi\dot{\phi} + \Delta_\phi}{J_x} \end{aligned} \quad (39)$$

Then, Eqs. (34) and (35) can be rewritten as

$$\begin{aligned} \dot{w}_{i,1} &= w_{i,2} \\ \dot{w}_{i,2} &= \Pi_i(t) + \sigma_i(t) \end{aligned} \quad (40)$$

where $i = 1, \cdots, 6$. Based on Assumption 1, uncertainties $\sigma_i(t)$, $i = 1, ..., 6$, have the following dynamics:

$$\dot{\sigma}_i(t) = c_{\sigma i}(t) \quad (41)$$

In fact, this assumption is satisfied with aircraft dynamic systems.

Let $w_{i,3} = \sigma_i(t)$, and $\dot{w}_{i,3} = \dot{\sigma}_i(t) = c_{\sigma i}(t)$, Eq. (40) can be augmented to

$$\begin{aligned} \dot{w}_{i,1} &= w_{i,2} \\ \dot{w}_{i,2} &= w_{i,3} + \Pi_i(t) \\ \dot{w}_{i,3} &= c_{\sigma i}(t) \end{aligned} \quad (42)$$

1) Integral-uncertainty observers for attitude estimation

Based on Theorem 1 or Corollary 1, the following corollary gives the design of integral-uncertainty observers for the jet aircraft.

Corollary 2: The integral-uncertainty observers are designed for aircraft attitude Eq. (35) as follows:

This article has been accepted for publication in a future issue of this journal, but has not been fully edited. Content may change prior to final publication. Citation information: DOI 10.1109/TAES.2017.2668078, IEEE Transactions on Aerospace and Electronic Systems

$$\begin{aligned}\dot{x}_{1,i,1} &= x_{1,i,2}\\ \dot{x}_{1,i,2} &= x_{1,i,3}+\Pi_i(t)\\ \varepsilon_i^4\dot{x}_{1,i,3} &= -k_{i,1}\left|\varepsilon_i x_{1,i,1}\right|^{\alpha_1} sign\left(x_{i,1}\right)\\ &\quad -k_{i,2}\left|x_{1,i,2}-w_{i,2}\right|^{\alpha_2} sign\left(x_{1,i,2}-w_{i,2}\right)\\ &\quad -k_{i,3}\left|\varepsilon_i^3 x_{1,i,3}\right|^{\alpha_3} sign\left(x_{1,i,3}\right)\end{aligned} \quad (43)$$

or

$$\begin{aligned}\dot{x}_{2,i,1} &= x_{2,i,2}\\ \dot{x}_{2,i,2} &= x_{2,i,3}+\Pi_i(t)\\ \varepsilon_i^4\dot{x}_{2,i,3} &= -k_{i,1}\varepsilon_i x_{2,i,1}-k_{i,2}\left(x_{2,i,2}-w_{i,2}\right)\\ &\quad -k_{i,3}\varepsilon_i^3 x_{2,i,3}\end{aligned} \quad (44)$$

where $i=4,5,6$. We can estimate $\Theta=(\psi,\theta,\phi)$ and the uncertainties, i.e., for $t\geq t_s$,

$$\begin{aligned}|x_{1,4,1}-\psi| &\leq L\varepsilon^{\alpha_1\gamma-1}, \left|x_{1,4,2}-\dot{\psi}\right|\leq L\varepsilon^{\alpha_1\gamma-2},\\ |x_{1,4,3}-\sigma_4(t)| &\leq L\varepsilon^{\alpha_1\gamma-3}, |x_{1,5,1}-\theta|\leq L\varepsilon^{\alpha_1\gamma-1},\\ \left|x_{1,5,2}-\dot{\theta}\right| &\leq L\varepsilon^{\alpha_1\gamma-2}, |x_{1,5,3}-\sigma_5(t)|\leq L\varepsilon^{\alpha_1\gamma-3},\\ |x_{1,6,1}-\phi| &\leq L\varepsilon^{\alpha_1\gamma-1}, \left|x_{1,6,2}-\dot{\phi}\right|\leq L\varepsilon^{\alpha_1\gamma-2},\\ |x_{1,6,3}-\sigma_6(t)| &\leq L\varepsilon^{\alpha_1\gamma-3}\end{aligned} \quad (45)$$

2) Augmented observers in [41] for velocity estimate in position dynamics

Based on [41], the following corollary gives the observers to estimate $(\dot{x},\dot{y},\dot{z})$ and uncertainties in the position dynamics in the jet aircraft.

Corollary 3: The augmented observers in [41] are designed for aircraft position Eq. (34) as follows:

$$\begin{aligned}\dot{x}_{i,1} &= x_{i,2}-\frac{k_{i,3}}{\varepsilon_i}\left|x_{i,1}-w_{i,1}\right|^{\alpha_3} sign(x_{i,1}-w_{i,1})\\ \dot{x}_{i,2} &= x_{i,3}-\frac{k_{i,2}}{\varepsilon_i^2}\left|x_{i,1}-w_{i,1}\right|^{\alpha_2} sign(x_{i,1}-w_{i,1})+\Pi_i(t)\\ \dot{x}_{i,3} &= -\frac{k_{i,1}}{\varepsilon_i^3}\left|x_{i,1}-w_{i,1}\right|^{\alpha_1} sign(x_{i,1}-w_{i,1})\end{aligned} \quad (46)$$

where $i=1,2,3$. From $X=(x,y,z)$, we can estimate $\dot{X}=(\dot{x},\dot{y},\dot{z})$ and $\sigma_i(t)$ $(i=1,2,3)$ by the above augmented observers, i.e., for $t\geq t_s$,

$$\begin{aligned}|x_{1,1}-x| &\leq L\varepsilon^{3\gamma}, |x_{1,2}-\dot{x}|\leq L\varepsilon^{3\gamma-1},\\ |x_{1,3}-\sigma_1(t)| &\leq L\varepsilon^{3\gamma-2}, |x_{2,1}-y|\leq L\varepsilon^{3\gamma},\\ |x_{2,2}-\dot{y}| &\leq L\varepsilon^{3\gamma-1}, |x_{2,3}-\sigma_2(t)|\leq L\varepsilon^{3\gamma-2},\\ |x_{3,1}-z| &\leq L\varepsilon^{3\gamma}, |x_{3,2}-\dot{z}|\leq L\varepsilon^{3\gamma-1},\\ |x_{3,3}-\sigma_3(t)| &\leq L\varepsilon^{3\gamma-2}\end{aligned} \quad (47)$$

If the attitude angle measurement is made by three encoders, the augmented observers in [41] can be selected to estimate the angular rates and the uncertainties in the attitude dynamics.

4.3 Controller design

In this section, a control law is derived for the purpose of attitude stabilization and trajectory tracking of the jet aircraft. The unknown states and uncertainties are reconstructed by the presented observers.

Suppose the reference trajectory and its finite order derivatives are bounded, and can be directly generated.

For the reference trajectory $X_d=(x_d,y_d,z_d)$, let $e_1=x-x_d$, $e_2=\dot{x}-\dot{x}_d$, $e_3=y-y_d$, $e_4=\dot{y}-\dot{y}_d$, $e_5=z-z_d$, and $e_6=\dot{z}-\dot{z}_d$, then the system error for position dynamics (34) is

$$\ddot{e}_p=m^{-1}(u_p+\Xi_p+\Omega_p+\Delta_p) \quad (48)$$

where

$$\begin{aligned}u_p &= \begin{bmatrix}u_{px}\\u_{py}\\u_{pz}\end{bmatrix}=\begin{bmatrix}c_\theta c_\psi\\c_\theta s_\psi\\-s_\theta\end{bmatrix}F_c, e_p=\begin{bmatrix}e_1\\e_3\\e_5\end{bmatrix},\\ \Delta_p &= \begin{bmatrix}\Delta_x\\\Delta_y\\\Delta_z\end{bmatrix},, \Xi_p=\begin{bmatrix}-m\ddot{x}_d\\-m\ddot{y}_d\\-m\ddot{z}_d-mg\end{bmatrix},\\ \Omega_p &= \begin{bmatrix}F_{wx}+F_{fx}+F_{vx}+F_{ex}\\F_{wy}+F_{fy}+F_{vy}+F_{ey}\\F_{wz}+F_{fz}+F_{vz}+F_{ez}\end{bmatrix}\end{aligned} \quad (49)$$

For the desired attitude angle $\Theta_d=(\psi_d,\theta_d,\phi_d)$, let $e_7=\psi-\psi_d$, $e_8=\dot{\psi}-\dot{\psi}_d$, $e_9=\theta-\theta_d$, $e_{10}=\dot{\theta}-\dot{\theta}_d$, $e_{11}=\phi-\phi_d$, $e_{12}=\dot{\phi}-\dot{\phi}_d$, then the system error for attitude dynamics (35) is

$$\ddot{e}_a=J^{-1}(u_a+\Xi_a+\Omega_a+\Delta_a) \quad (50)$$

where

$$\begin{aligned}e_a &= \begin{bmatrix}e_7\\e_9\\e_{11}\end{bmatrix},\Omega_a=\begin{bmatrix}\dot{\theta}\dot{\phi}(J_x-J_y)\\\dot{\psi}\dot{\phi}(J_z-J_x)\\\dot{\psi}\dot{\theta}(J_y-J_z)\end{bmatrix},\\ \Xi_a &= \begin{bmatrix}-J_z\ddot{\psi}_d\\-J_y\ddot{\theta}_d\\-J_x\ddot{\phi}_d\end{bmatrix},\Delta_a=\begin{bmatrix}\Delta_\psi-k_\psi\dot{\psi}\\\Delta_\theta-k_\theta\dot{\theta}\\\Delta_\phi-k_\phi\dot{\phi}\end{bmatrix},\\ u_a &= \begin{bmatrix}\tau_\psi\\\tau_\theta\\\tau_\phi\end{bmatrix},J=\begin{bmatrix}J_z&0&0\\0&J_y&0\\0&0&J_x\end{bmatrix}\end{aligned} \quad (51)$$

1) Controller design for position dynamics

Theorem 2: For position dynamics (34), to track the reference trajectory $X_d=(x_d,y_d,z_d)$, if the controller is designed as

$$u_p=-\Xi_p-\Omega_p-\widehat{\Delta}_p-m(k_{p1}\widehat{e}_p+k_{p2}\widehat{\dot{e}}_p) \quad (52)$$

where $\widehat{e}_1=\widehat{x}-x_d$, $\widehat{e}_2=\widehat{\dot{x}}-\dot{x}_d$, $\widehat{e}_3=\widehat{y}-y_d$, $\widehat{e}_4=\widehat{\dot{y}}-\dot{y}_d$, $\widehat{e}_5=\widehat{z}-z_d$, $\widehat{e}_6=\widehat{\dot{z}}-\dot{z}_d$; $k_{p1},k_{p2}>0$, and

$$\widehat{e}_p=\begin{bmatrix}\widehat{e}_1\\\widehat{e}_3\\\widehat{e}_5\end{bmatrix},\widehat{\dot{e}}_p=\begin{bmatrix}\widehat{e}_2\\\widehat{e}_4\\\widehat{e}_6\end{bmatrix} \quad (53)$$

This article has been accepted for publication in a future issue of this journal, but has not been fully edited. Content may change prior to final publication. Citation information: DOI 10.1109/TAES.2017.2668078, IEEE Transactions on Aerospace and Electronic Systems

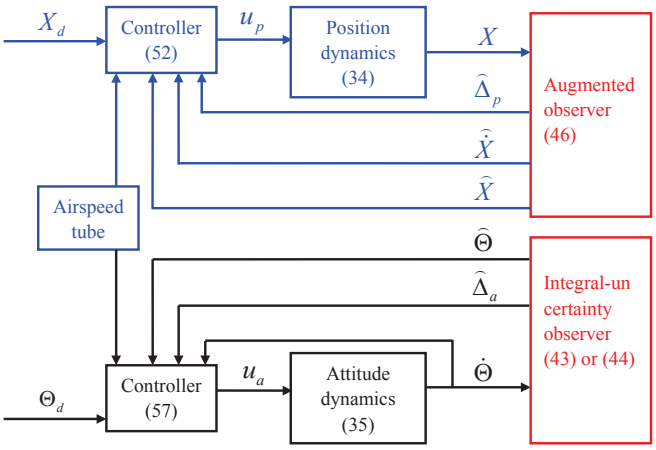

Fig. 5. Control of position and attitude dynamics.

the control system is described in Fig.5, then the position error dynamic system (48) rendering by controller (52) will converge asymptotically to the origin, i.e., the tracking errors $e_p \to 0$ and $\dot{e}_p \to 0$ as $t \to \infty$.

Proof: In the light of Corollary 3, for $t \geq ts = \varepsilon\Gamma$, the observation signals $\left\|\widehat{X} - X\right\| \leq L\varepsilon^{3\gamma}$, $\left\|\widehat{\dot{X}} - \dot{X}\right\| \leq L\varepsilon^{3\gamma-1}$, $\left\|\widehat{\Delta}_p - \Delta_p\right\| \leq L\varepsilon^{3\gamma-2}$. Considering controller (52), the closed-loop error system for the position dynamics is

$$\ddot{e}_p = -k_{p1}e_p - k_{p2}\dot{e}_p - k_{p1}(\widehat{X} - X) - k_{p2}(\widehat{\dot{X}} - \dot{X}) - (\widehat{\Delta}_p - \Delta_p) \tag{54}$$

For $t \geq \varepsilon\Gamma$ and sufficiently small ε, selecting the Lyapunov function be $V_1 = k_{p1}e_p^T e_p + \frac{1}{2}\dot{e}_p^T \dot{e}_p$, we can obtain that $e_p \to 0$ and $\dot{e}_p \to 0$ as $t \to \infty$. This concludes the proof. ■

From (49), we know that

$$F_c = \|u_p\|_2 = \sqrt{u_{px}^2 + u_{py}^2 + u_{pz}^2} \tag{55}$$

The desired pitch and yaw angles are, respectively,

$$\theta_d = -\arcsin(\frac{u_{pz}}{F_c}), \psi_d = \begin{cases} \arctan(\frac{u_{py}}{u_{px}}), u_{px} \neq 0 \\ \pi/2, u_{px} = 0 \text{ and } \dot{x}_d > 0 \\ 3\pi/2, u_{px} = 0 \text{ and } \dot{x}_d < 0 \end{cases} \tag{56}$$

and the desired roll angle ϕ_d can be set to a reference value.

2) Controller design for attitude dynamics

Theorem 3: For attitude dynamics (35), to track the desired attitude $\Theta_d = (\psi_d, \theta_d, \phi_d)$, if the controller is designed as

$$u_a = -\Xi_a - \Omega_a - \widehat{\Delta}_a - J[k_{a1}\widehat{e}_a + k_{a2}\dot{e}_a + L_c sign(\dot{e}_a)] \tag{57}$$

where, $k_{a1}, k_{a2}, L_c > 0$; $\widehat{e}_7 = \widehat{\psi} - \psi_d$, $\widehat{e}_9 = \widehat{\theta} - \theta_d$, $\widehat{e}_{11} = \widehat{\phi} - \phi_d$; $\widehat{e}_a = \begin{bmatrix} \widehat{e}_7 & \widehat{e}_9 & \widehat{e}_{11} \end{bmatrix}^T$; $\dot{e}_a = \begin{bmatrix} e_8 & e_{10} & e_{12} \end{bmatrix}^T$; and the control system is described in Fig.5, then the attitude error dynamic system (50) rendering by controller (57) will converge asymptotically to the origin, i.e., the tracking errors $e_a \to 0$ and $\dot{e}_a \to 0$ as $t \to \infty$.

Proof: In the light of Corollary 2, for $t \geq ts = \varepsilon\Gamma$, the observation signals $\left\|\widehat{\Theta} - \Theta\right\| \leq L\varepsilon^{\alpha_1\gamma-1}$ and $\left\|\widehat{\Delta}_a - \Delta_a\right\| \leq L\varepsilon^{\alpha_1\gamma-3}$. Considering controller (57), the closed-loop error system for the attitude dynamics is

$$\ddot{e}_a = -k_{a1}e_a - k_{a2}\dot{e}_a - L_c sign(\dot{e}_a) - k_{a1}(\widehat{\Theta} - \Theta) - (\widehat{\Delta}_a - \Delta_a) \tag{58}$$

For $t \geq \varepsilon\Gamma$ and sufficiently small ε, selecting the Lyapunov function be $V_2 = k_{a1}e_a^T e_a + \frac{1}{2}\dot{e}_a^T \dot{e}_a$, we can obtain that $e_a \to 0$ and $\dot{e}_a \to 0$ as $t \to \infty$. This concludes the proof. ■

V. Computational Analysis and Simulations

In this section, we use a simulation on the jet aircraft to illustrate the effectiveness of the proposed estimate and control methods. The goal is to force the aircraft to track a reference trajectory. Here, the aircraft tracks a given trajectory (x_d, y_d, z_d) without the information of ($\dot{x}$, $\dot{y}$, $\dot{z}$, ψ, θ, ϕ, d_1, d_2, d_3, d_4, d_5, d_6). The estimation performances of the presented integral-uncertainty observers are compared with Kalman filter [14].

In this simulation, without the information of velocity, attitude angle and uncertainties, the aircraft is controlled to track the reference trajectory. The position is obtained from the GPS receiver, and the altitude information is from the altimeter. The angular velocity $(\dot{\psi}, \dot{\theta}, \dot{\phi})$ is measured by the IMU. The integral-uncertainty observer (43) (or (44)) is used to estimate the attitude angle (ψ, θ, ϕ) and uncertainties (d_4, d_5, d_6) in the attitude dynamics from the angular velocity $(\dot{\psi}, \dot{\theta}, \dot{\phi})$. The augmented observer (46) is adopted to estimate the velocity $(\dot{x}, \dot{y}, \dot{z})$ and uncertainties (d_1, d_2, d_3) in the position dynamics from the position (x, y, z). Controllers (52) and (57) are presented to stabilize the flight dynamics. Reference trajectory: The given waypoints generate the reference trajectory (x_d, y_d, z_d) shown in Fig.6.

The initial states of aircraft are: ($x(0)$, $\dot{x}(0)$, $y(0)$, $\dot{y}(0)$, $z(0)$, $\dot{z}(0)$, $\psi(0)$, $\dot{\psi}(0)$, $\theta(0)$, $\dot{\theta}(0)$, $\phi(0)$, $\dot{\phi}(0)$) = (0, 0, 0, 0, 0, 0, 0, 0, 0, 0, 0, 0); the initial states of the observers are: ($x_{1,1}(0)$, $x_{1,2}(0)$, $x_{1,3}(0)$, $x_{2,1}(0)$, $x_{2,2}(0)$, $x_{2,3}(0)$, $x_{3,1}(0)$, $x_{3,2}(0)$, $x_{3,3}(0)$, $x_{4,1}(0)$, $x_{4,2}(0)$, $x_{4,3}(0)$, $x_{5,1}(0)$, $x_{5,2}(0)$, $x_{5,3}(0)$, $x_{6,1}(0)$, $x_{6,2}(0)$, $x_{6,3}(0)$) = (0 0, 0, 0, 0, 0, 0, 0, 0, 0, 0.2, 0.3, 0, 0.3, −0.1, 0, 0.2, −0.2, 0). Let the uncertainties be: $\Delta_x = 0.5\sin(t)$, $\Delta_y = 0.5\sin(t)$, $\Delta_z = 0.5\sin(t)$, $\Delta_\psi = 0.2\sin(0.8t)$, $\Delta_\theta = 0.2\sin(0.8t)$, $\Delta_\phi = 0.2\sin(0.8t)$.

The position measurement outputs are $y_{opi} = w_{i,1} + n_i$, where $i = 1, 2, 3$, and $w_{1,1} = x$, $w_{2,1} = y$, $w_{3,1} = z$; the attitude measurement outputs are $y_{opi} = w_{i,2} + n_i$, where $i = 4, 5, 6$, and $w_{4,2} = \dot{\psi}$, $w_{5,2} = \dot{\theta}$, $w_{6,2} = \dot{\phi}$; n_i (where $i = 1, \cdots, 6$) are the disturbances.

The disturbances n_i (where $i = 1, \cdots, 6$) include two types of noises: Random number with Mean=0, Variance=0.001, Initial speed=0, and Sample time=0; Pulses with Amplitude=0.001, Period=1s, Pulse width=1, and Phase delay=0.

The aerodynamic parameters of the unmanned jet aircraft were obtained through the wind tunnel tests. The parameters are given as follows:

Jet aircraft: $m = 35.6kg$, $g = 9.8m/s^2$, wingspan=1.92m, wing area=1.58m^2, Fuselage length=2.35m, and $C_{L10} = C_{L20} = 0.3145$, $C_{L1\alpha} = C_{L2\alpha} = 0.5122$, $C_{1\dot{\phi}} = C_{2\dot{\phi}} = 0.1183$, $C_{L\delta1} = C_{L\delta2} = 0.1634$, $C_{D10} = C_{D20} = 0.0083$,

This article has been accepted for publication in a future issue of this journal, but has not been fully edited. Content may change prior to final publication. Citation information: DOI 10.1109/TAES.2017.2668078, IEEE Transactions on Aerospace and Electronic Systems

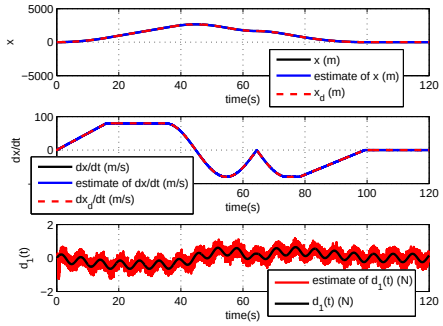

(a)

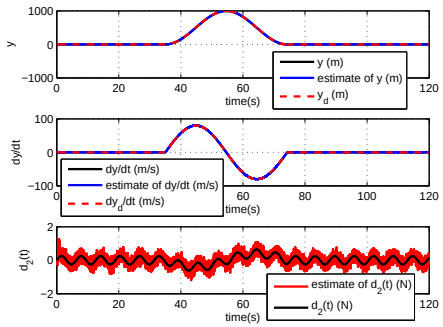

(b)

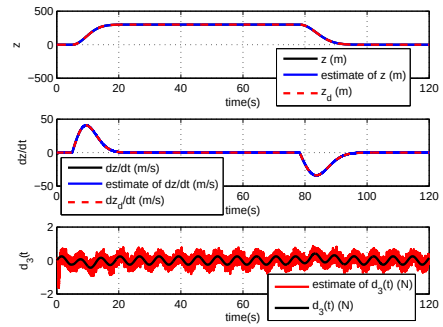

(c)

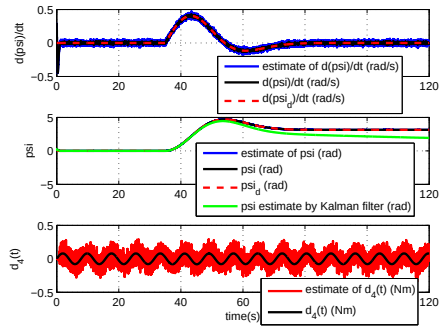

(d)

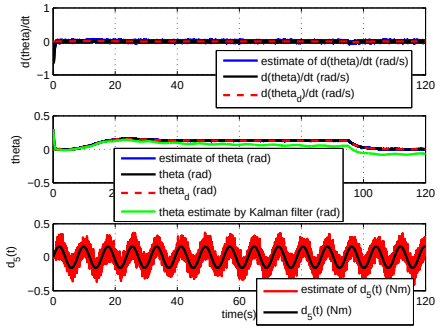

(e)

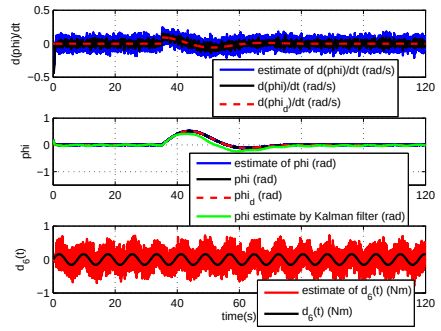

(f)

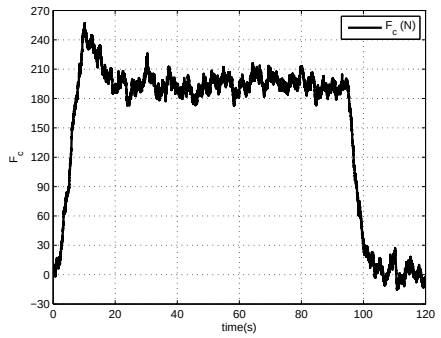

(g)

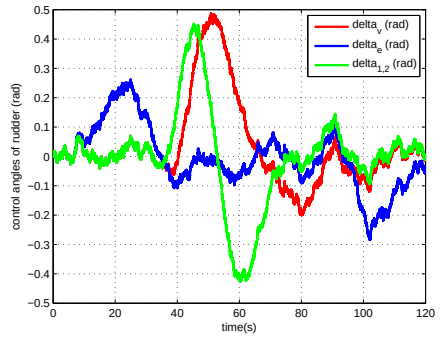

(h)

Fig. 6. Aircraft control based on nonlinear integral-uncertainty observer. (a) Estimation in x coordinate. (b) Estimation in y coordinate. (c) Estimation in z coordinate. (d) Estimation in yaw dynamics.

Fig. 6. (continued): Aircraft control based on nonlinear integral-uncertainty observer. (e) Estimation in pitch dynamics. (f) Estimation in roll dynamics. (g) Thrust force. (h) Control angles of rudder.

This article has been accepted for publication in a future issue of this journal, but has not been fully edited. Content may change prior to final publication. Citation information: DOI 10.1109/TAES.2017.2668078, IEEE Transactions on Aerospace and Electronic Systems

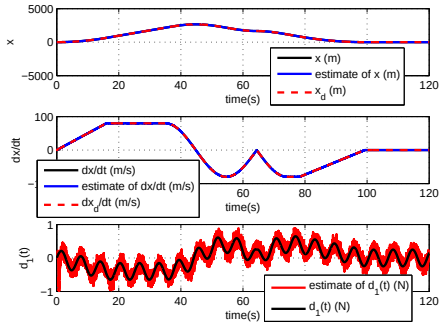

(a)

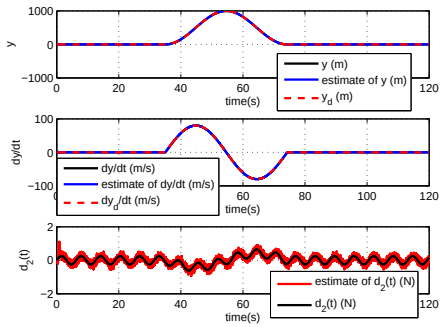

(b)

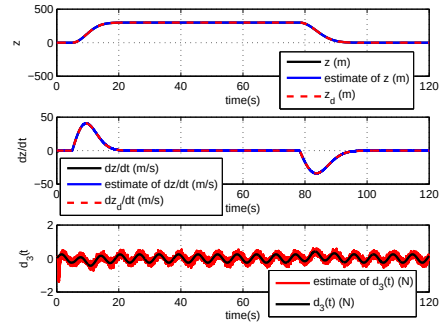

(c)

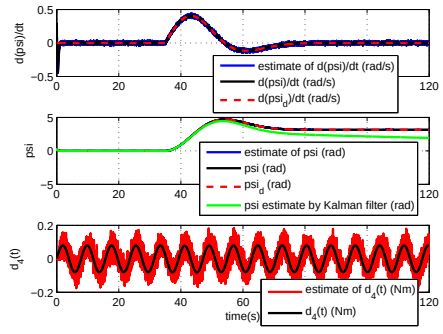

(d)

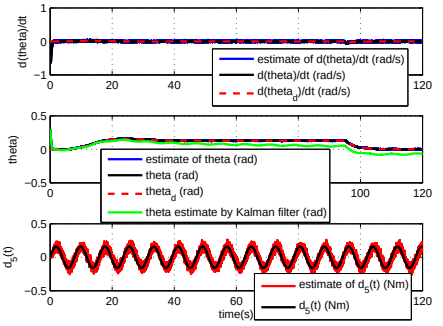

(e)

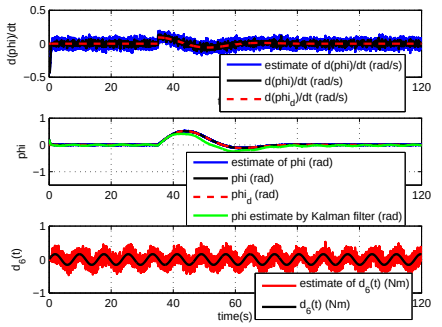

(f)

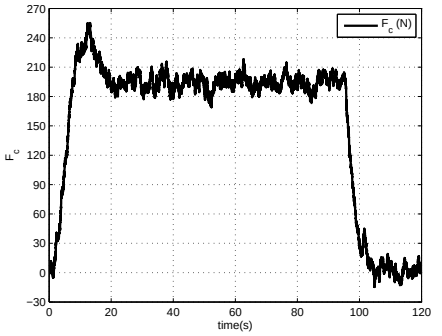

(g)

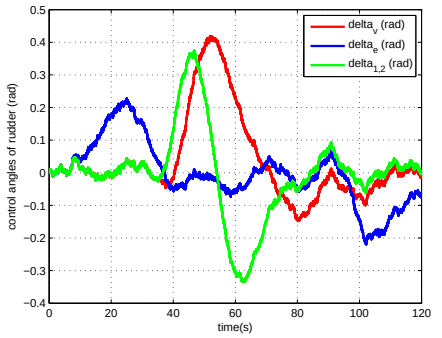

(h)

Fig. 7. Aircraft control based on linear integral-uncertainty observer. (a) Estimation in x coordinate. (b) Estimation in y coordinate. (c) Estimation in z coordinate. (d) Estimation in yaw dynamics.

Fig.7. (continued): Aircraft control based on linear integral-uncertainty observer. (e) Estimation in pitch dynamics. (f) Estimation in roll dynamics. (g) Thrust force. (h) Control angles of rudder.

This article has been accepted for publication in a future issue of this journal, but has not been fully edited. Content may change prior to final publication. Citation information: DOI 10.1109/TAES.2017.2668078, IEEE Transactions on Aerospace and Electronic Systems

$C_{1\dot{\psi}} = C_{2\dot{\psi}} = 0.0057$, $C_{L30} = C_{L40} = 0.3029$, $C_{L3\alpha} = C_{L4\alpha} = 0.4753$, $C_{4\dot{\phi}} = C_{4\dot{\phi}} = 0.1067$, $C_{L\delta3} = C_{L\delta4} = 0.1446$, $C_{D30} = C_{D40} = 0.0062$, $C_{3\dot{\psi}} = C_{4\dot{\psi}} = 0.0034$; $C_{l5\alpha} = 0.0812$, $C_{d50} = 0.0063$, $C_{d5\alpha} = 0.0094$, $J_x = 18Nm$, $J_y = 18Nm$, $J_z = 34Nm$, $k_\psi = k_\theta = k_\phi = 0.52Ns/rad$;

Augmented observer: $k_{i,1} = 6$, $k_{i,2} = 11$, $k_{i,3} = 6$, $\varepsilon_1 = 0.2$, $\alpha_{i,1} = 0.8$, $i = 1, 2, 3$;

Nonlinear integral-uncertainty observer: $k_{1,i,1} = 0.1$, $k_{1,i,2} = 2$, $k_{1,i,3} = 1$, $\varepsilon_{1,2} = 1/3$, $\alpha_{i,3} = 0.3$, $i = 4, 5, 6$;

Linear integral-uncertainty observer: $k_{2,i,1} = 0.1$, $k_{2,i,2} = 2$, $k_{2,i,3} = 1$, $\varepsilon_{2,2} = 1/3$, $i = 4, 5, 6$;

Controllers: $k_{p1} = 3.2$, $k_{p2} = 1.6$, $k_{a1} = 1.5$, $k_{a2} = 1.0$, $L_c = 0.15$.

The sampling time is $1ms$. The data of flying test were presented in Figs.6 and 7. Fig.6 shows the aircraft control based on nonlinear integral-uncertainty observer. Fig. 6(a) describes the estimate of x, dx/dt and $d_1(t)$; Fig. 6(b) describes the estimate of y, dy/dt and $d_2(t)$; Fig. 6(c) presents the estimate of z, dz/dt and $d_3(t)$; Fig. 6(d) presents the estimate of the yaw angle ψ, yaw rate $d\psi/dt$ and $d_4(t)$; Fig. 6(e) presents the estimate of the pitch angle θ, pitch rate $d\psi/dt$ and $d_5(t)$; Fig. 6(f) presents the estimate of the roll angle ϕ, roll rate $d\phi/dt$ and $d_1(t)$; Figs. 6(g) and 6(h) present the controller curves of F_c, δ_v, δ_e and $\delta_{1,2}$, respectively. Fig.7 presents the aircraft control based on linear integral-uncertainty observer. In the simulation figures, the green lines denote measured values, the blue lines are the estimated values, and the red dot lines are the desired lines. In the Figs. 6 and 7, high-frequency noise and the bounded uncertainties exist. Position tracking, the estimations of velocity, attitude angle and the uncertainties are described, respectively. Black lines are the real values, blue lines are the estimated values, and the red dot lines are the desired values. In the simulation above, although high-frequency stochastic noises exist in the measurement signals, the uncertainties exist in the aircraft dynamics, and only the angular velocities are considered in the IMU outputs, the attitude estimations by the presented integral-uncertainty observer, the velocity-uncertainty estimations by the augmented observer and the control results by the designed controller have satisfying qualities. The stochastic noises are rejected sufficiently by the observers.

Figs. 6 and 7 also describe the estimation comparisons of attitude estimations by the integral-uncertainty observers and Kalman filter. From Figs. Figs. 6 (d), (e), (f) and Figs. 7 (d), (e), (f), the obvious estimation drifts of attitude angles exist by Kalman filter. Furthermore, from Figs.6 and 7, no drift phenomena happen for the integral-uncertainty observers. In the tracking outputs, not only the dynamical performances are fast, but also the tracking precisions are accurate.

We found that, for the simulation computational environment, the nonlinear and linear integral-uncertainty observers can obtain almost the same estimate performances.

VI. Experimental Verification of the Proposed Observers on the Unmanned Jet Aircraft

In this section, in order to verify the effectiveness of the proposed observation algorithms and controller proposed in the previous sections, we present a real-time experiment on the flight of an unmanned jet aircraft. The jet aircraft prototype has been designed and shown in Fig.2. In the aircraft, a jet engine (JetCat P200-SX) is adopted to provide the thrust, and its starter includes: Jet-tronic ECU (fuel control electronics); electronic valve; electronic starting gas valve; electronic fuel valve; fuel tubing, tubing connector set, filters, and cable set; 2 cell, 3300mA LiPoly battery pack; starting gas tank. The thrust is 220 N (52 lbs) @ 112000 RPM, and RPM range: 33000 $\sim$ 112000 RPM. An IMU (XsensMTI AHRS) is used to measure the angular velocity, whose sampling frequency is 10 kHz. Arduino Mega 2560 (sampling frequency: 16MHz) $\rightarrow$ (CPU clock rate (or speed)): 16MHz. Gumstix microcomputer and an Arduino Mega 2560 are taken as the driven boards, which have multiple PWM output channels (See Fig.8). The input voltage is 7 $\sim$ 12V. The control update time is 5ms. The rudders (FUTABA S3001) are adopted to control the bias angles of elevators, verticals and ailerons, respectively. GPS MT3329 (10Hz update rate) is selected as the GPS receiver. A VTI Technologies SCP1000 altimeter with 10 cm resolution is utilized for above the sea level altitude measurements at higher altitudes, and its sampling frequency is 9 Hz. A SF02-F laser altimeter is used for altitude measurements at lower altitudes with 40 m range (sampling frequency: 12 Hz), and it is fine for landings. A kpilot 32 digital air speed sensor is utilized to obtain the relative wind speed (sampling frequency: 192 kHz). A 4239-01 AOA sensor is used to measure the angle of attack (sampling frequency: 100 kHz). The flight control system implementation on the hardware is shown in Fig.8.

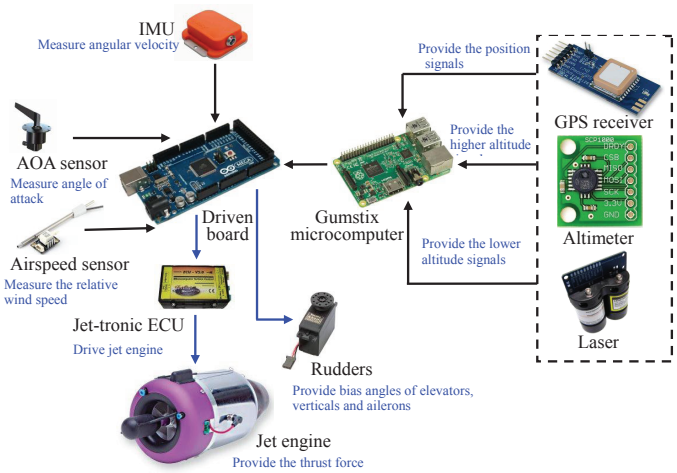

Fig. 8. Flight control system implementation on the hardware.

The aerodynamic parameters of the unmanned jet aircraft were obtained through the wind tunnel tests. The parameters have been given in the section of simulation. Here, the discrete forms of the observers use the 4th-order Runge–Kutta Method. The presented method is suitable to the several sampling times (i.e., 0.001 in the simulation and 0.005 in the experiment, respectively). The discrete-form analysis of a similar continuous differentiator has been described in [12].

In this experiment, without the information of velocity, attitude angle and uncertainties, the unmanned jet aircraft is

This article has been accepted for publication in a future issue of this journal, but has not been fully edited. Content may change prior to final publication. Citation information: DOI 10.1109/TAES.2017.2668078, IEEE Transactions on Aerospace and Electronic Systems

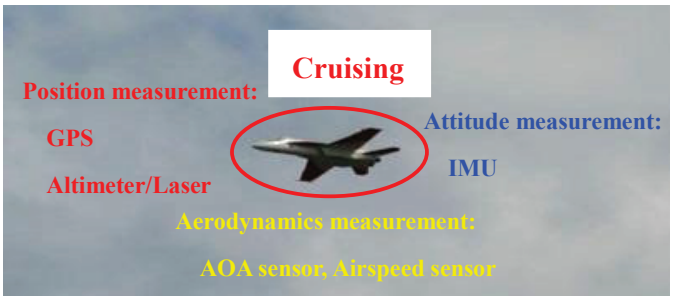

Fig. 9. Flight test for jet aircraft.

controlled to track the reference trajectory. The position is obtained from the GPS receiver, and the altitude information is from the altimeter. The angular velocity $(\dot{\psi}, \dot{\theta}, \dot{\phi})$ is measured by the IMU.

Integral-uncertainty observer (43) (or (44)) is used to estimate the attitude angle (ψ, θ, ϕ) and uncertainties in the attitude dynamics from the angular velocity $(\dot{\psi}, \dot{\theta}, \dot{\phi})$. The augmented observer (46) is adopted to estimate the velocity $(\dot{x}, \dot{y}, \dot{z})$ and uncertainties in the position dynamics from the position (x, y, z). Controllers (52) and (57) are designed to control the jet aircraft to track the reference trajectory.

The flying test scenario for the jet aircraft is shown in Fig.9, and the data of flying test are presented in Figs.10, 11, 12 and 13. In Fig.10, Fig.10(a) shows the trajectory tracking for the unmanned jet aircraft. Fig.10(b) describes the position estimate in x-direction; Fig.10(c) describes the position estimate in y-direction; Fig.10(d) describes the position estimate in z-direction. In Fig.11, Fig.11(a) describes the velocity estimate in x-direction; Fig.11(b) describes the velocity estimate in y-direction; Fig.11(c) describes the velocity estimate in z-direction. The attitude angles estimate by the integral-uncertainty observers are shown in Fig.12, where Fig.12(a) shows the yaw angle estimate; Fig.12(b) shows the pitch angle estimate; Fig.12(c) shows the roll angle estimate. Fig. 13 presents the controller curves of the thrust force F_c and the duty ratios of rudders control δ_v, δ_e and $\delta_{1,2}$, respectively. The pulse control of the rudder is shown in Table 2 (The time period is $20ms$).

Duty ratio	Pulse width	output angle
0.025	$0.5(ms)$	$-90°$
0.05	$1(ms)$	$-45°$
0.075	$1.5(ms)$	$0°$
0.1	$2(ms)$	$45°$
0.125	$2.5(ms)$	$90°$

Table 2 Pulse control of rudder

In the experiment above, although the stochastic noise exists in the GPS signal, the uncertainties exist in the aircraft dynamics, and only the angular velocity is considered in the IMU output, the attitude estimations by the presented integral-uncertainty observer, the velocity-uncertainty estimations by our previous augmented observer [41] and the control results by the designed controller have satisfying qualities. The estimation results of attitude angles are satisfying and are better than those of IMU (XsensMTI AHRS) (See Fig.12).

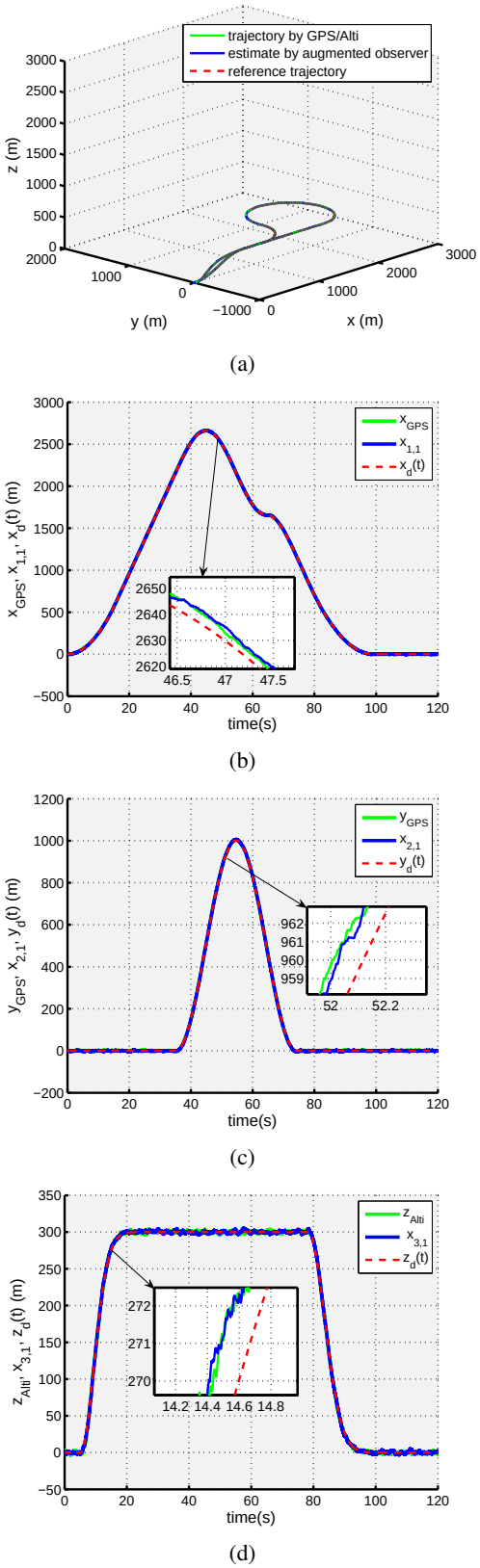

Fig. 10. Position navigation. (a) Position trajectory. (b) Position in x-direction. (c) Position in y-direction. (d) Position in z-direction.

This article has been accepted for publication in a future issue of this journal, but has not been fully edited. Content may change prior to final publication. Citation information: DOI 10.1109/TAES.2017.2668078, IEEE Transactions on Aerospace and Electronic Systems

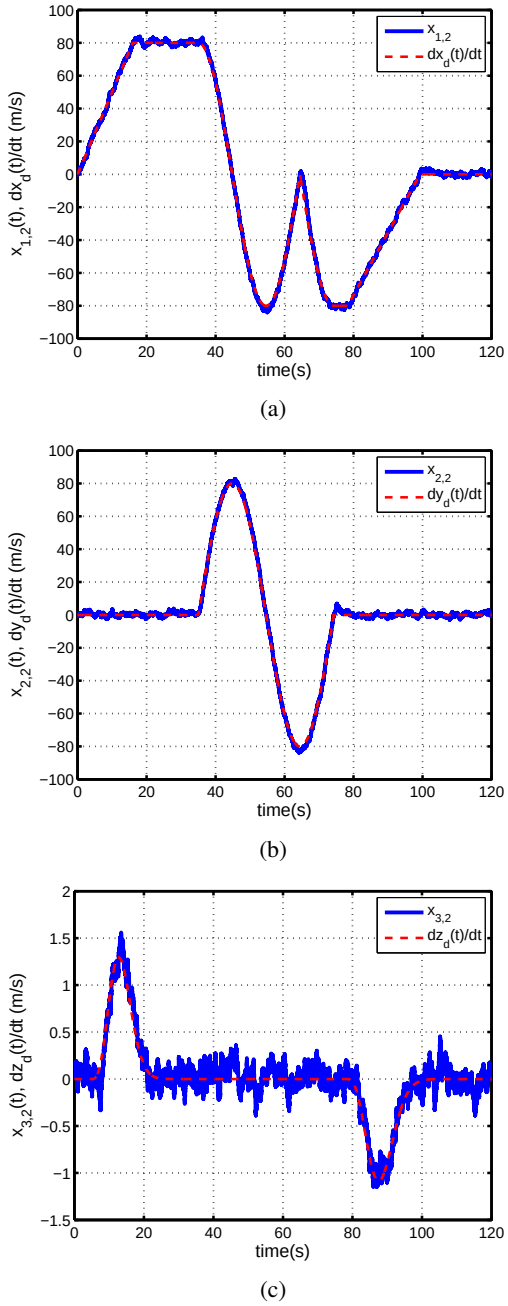

Fig. 11. Velocity estimate by augmented observer (46). (a) Velocity in x-direction. (b) Velocity in y-direction. (c) Velocity in z-direction.

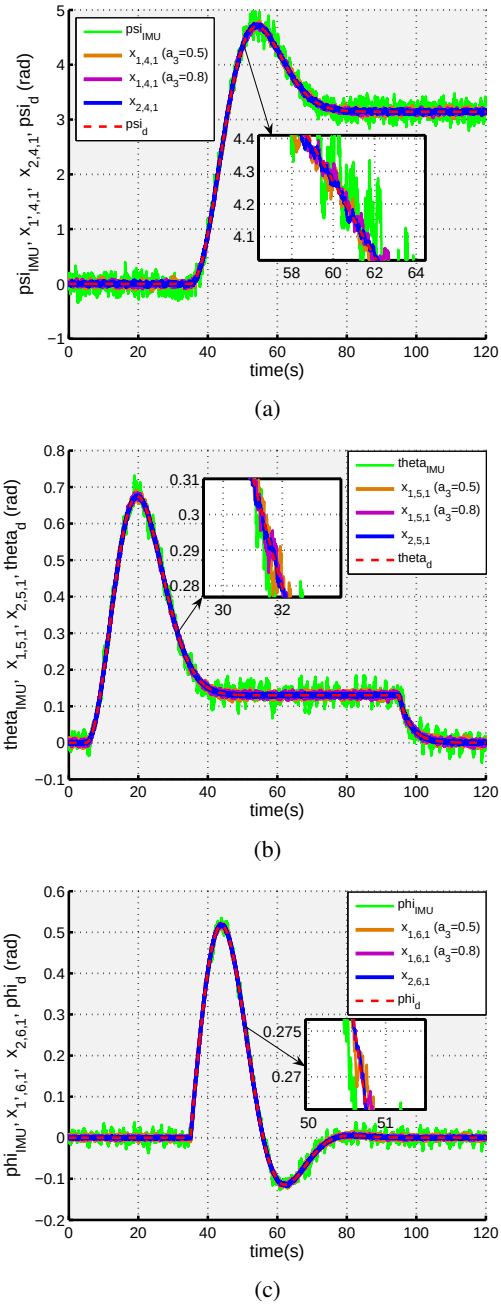

Fig. 12. Attitude angles estimate by integral-uncertainty observers (43) and (44). (a) Yaw angle estimate. (b) Pitch angle estimate. (c) Roll angle estimate.

Furthermore, no drift phenomena happen, and trajectory taking are accurate. From Fig.12, we also found that, the linear integral-uncertainty observer ($\alpha_3 = 1$) can obtain the better estimate results than those of nonlinear one ($\alpha_3 = 0.5, 0.8$). It is more easier to regulate the parameters of the linear integral-uncertainty observer. The linear observer is more suitable to the existing hardware computational environment in the aircraft system, and it exhibited more satisfying estimate performances.

VII. Conclusions

In this paper, two types of integral-uncertainty observers have been developed, which all can estimate the integral state of measurement output signal and the uncertainty in system, synchronously. The effectiveness of the proposed integral-uncertainty observers was shown by the simulations and experiments on an unmanned jet aircraft: i) they succeeded in estimating the attitude angle and uncertainties in attitude dynamics from the angular velocity measurement; ii) The flying test also verified the validity of our previous augmented observer, which estimated the velocity and uncertainties in

This article has been accepted for publication in a future issue of this journal, but has not been fully edited. Content may change prior to final publication. Citation information: DOI 10.1109/TAES.2017.2668078, IEEE Transactions on Aerospace and Electronic Systems

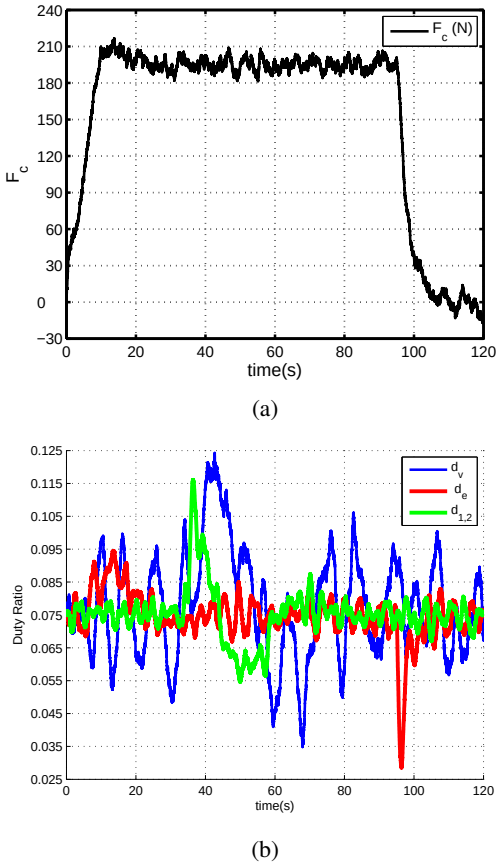

Fig. 13. Controllers. (a) Thrust force. (b) Duty ratios of rudders control.

position from the GPS receiver signals. iii) The satisfying estimate precision and the strong robustness of the integral-uncertainty observers make the selected control law very simple. The merits of the presented integral-uncertainty observers include the synchronous estimation of attitude angles and uncertainties, ease of parameters selection, sufficient stochastic noise rejection and almost no drift phenomenon. Although high-frequency stochastic noises and measurement errors exist, the attitude angle and uncertainty estimations by the presented observers and the tracking results by the designed controller have satisfying qualities. Moreover, due to the limitation of hardware computational environment and the requirement of ease of parameters regulation, the proposed linear integral-uncertainty observer can obtain the better estimate results than those of the nonlinear one. Our future work is to optimize the parameters of the presented methods.

ACKNOWLEDGEMENT

This work is partially supported by Research Grants Council, Hong Kong, SAR PR China under RGC16205115.

APPENDIX A

The related concepts of finite-time stability of autonomous systems are presented here.

Definition 1 in [37]: Let us consider a time-invariant system in the form of

$$\dot{x} = f(x), f(0) = 0, x \in R^n, \tag{59}$$

where $f : D \to R^n$ is continuous on open neighborhood $D \subseteq R^n$ of the origin. The origin is said to be a finite-time-stable equilibrium of the above system if there exists an open neighborhood $N \subseteq D$ of the origin and a function $T_f : N\backslash\{0\} \to (0, \infty)$, called the settling-time function, such that the following statements hold: (i) Finite-time-convergence: For every $x \in N\backslash\{0\}$, ψ^x is the flow starting from x and defined on $[0, T_f(x))$, $\psi^x(t) \in N\backslash\{0\}$ for all $t \in [0, T_f(x))$, and $\lim_{t\to T_f(x)} \psi^x(t) = 0$.

(ii) Lyapunov stability: For every open neighborhood U_ε of 0 there exists an open subset U_δ of N containing 0 such that, for every $x \in U_\delta\backslash\{0\}$, $\psi^x(t) \in U_\varepsilon$ for all $t \in [0, T_f(x))$.

The origin is said to be a globally finite-time-stable equilibrium if it is a finite-time-stable equilibrium with $D = N = R^n$. Then the system is said to be finite-time-convergent with respect to the origin.

Assumption in [11]: For a system depicted by Eq. (59), there exists $\rho_i \in (0, 1], i = 1, \cdots, n$, and a nonnegative constant $\overline{a}$ such that

$$\left|f_j(\widetilde{z}_1, \cdots, \widetilde{z}_n) - f_j(\overline{z}_1, \cdots, \overline{z}_n)\right| \le \overline{a} \sum_{i=1}^{n} |\widetilde{z}_i - \overline{z}_i|^{\rho_i} \tag{60}$$

where $\widetilde{z}_i, \overline{z}_i \in R, i = 1, \cdots, n$, $j = 1, \cdots, n$.

There are many nonlinear functions capable of satisfying this assumption. For example, one such function is x^{ρ_i} since $|x^{\rho_i} - \overline{x}^{\rho_i}| \le 2^{1-\rho_i} |x - \overline{x}|^{\rho_i}, \rho_i \in (0, 1]$.

Theorem 4.2 in [37]: Suppose there exists a continuous function $V : R^n - R$ such that the following conditions holds:

(i) V is positive definite;

(ii) There exist real numbers $c > 0$ and $\beta_c \in (0, 1)$ such that

$$\dot{V}(x) + c(V(x))^{\beta_c} \le 0 \tag{61}$$

Then (59) is globally finite-time stable. Moreover, if N is as in Definition 1 and T_f is the setting time function, then

$$T_f(x) \le \frac{1}{c(1-\beta_c)} V(x)^{1-\beta_c} \tag{62}$$

Proposition 8.1 in [38]: Let $k_1, \cdots, k_n > 0$ be such that $s^n + k_n s^{n-1} + \cdots + k_2 s + k_1$ is Hurwitz, and consider the system

$$\begin{aligned} \dot{x}_i &= x_{i+1}; i = 1, \cdots, n-1, \\ \dot{x}_n &= -\sum_{i=1}^{n} k_i |x_i|^{\alpha_i} sign(x_i) \end{aligned} \tag{63}$$

there exists $\xi_c \in (0, 1)$ such that, for every $\alpha \in (1 - \xi_c, 1)$, the origin is globally finite-time-stable equilibrium for Eq. (63) where $\alpha_1, \cdots, \alpha_n$ satisfy

$$\alpha_{i-1} = \frac{\alpha_i \alpha_{i+1}}{2\alpha_{i+1} - \alpha_i}, i = 2, \cdots, n \tag{64}$$

with $\alpha_{n+1} = 1$ and $\alpha_n = \alpha$.

This article has been accepted for publication in a future issue of this journal, but has not been fully edited. Content may change prior to final publication. Citation information: DOI 10.1109/TAES.2017.2668078, IEEE Transactions on Aerospace and Electronic Systems

Theorem 5.2 in [37]: Consider the perturbed system of (59) following:

$$\dot{x} = f(x) + g(t, x(t)), x(0) = x_0 \tag{65}$$

suppose there exists a function $V : D \to R$ such that V is positive definite and Lipschitz continuous on D, and satisfies (61), where $\nu \subseteq D$ is an open neighborhood of the origin, $c > 0$ and $\beta_c \in (0, \frac{1}{2})$. Then there exist $\delta_0 > 0$, $\mu > 0$, $\Gamma > 0$, and an open neighborhood U of origin such that, for every continuous function $g : R_+ \times D \to R^n$ with

$$\delta = \sup_{R_+ \times D} \|g(t, x(t))\| \leq \delta_0 \tag{66}$$

every right maximally defined solution x of (65) with $x(0) \in U$ is defined on R_+ and satisfies $x(t) \in U$ for all $t \in R_+$ and

$$\|x(t)\| \leq \mu \delta^{\gamma}, t \geq \Gamma \tag{67}$$

where $\gamma = (1 - \beta_c)/\beta_c > 1$.

APPENDIX B

Proof of Theorem 1: The system error between Eqs. (5) and (4) is given by:

$$\begin{aligned}
\dot{e}_1 &= e_2; \dot{e}_2 = e_3; \\
\varepsilon_3^4 \dot{e}_3 &= -k_1 |\varepsilon e_1 + \varepsilon w_1(t)|^{\alpha_1} sign(e_1 + w_1(t)) \\
&\quad - \frac{k_2}{\varepsilon^{2\alpha_2}} \left|\varepsilon^2 e_2 - \varepsilon^2 d(t)\right|^{\alpha_2} sign(e_2 - d(t)) \\
&\quad - k_3 \left|\varepsilon^3 e_3 + \varepsilon^3 w_3(t)\right|^{\alpha_3} sign(e_3 + w_3(t)) \\
&\quad - \varepsilon^4 c_\sigma(t)
\end{aligned} \tag{68}$$

Eq. (68) can be rewritten as:

$$\begin{aligned}
\frac{d\varepsilon e_1}{dt/\varepsilon} &= \varepsilon^2 e_2; \frac{d\varepsilon^2 e_2}{dt/\varepsilon} = \varepsilon^3 e_3; \\
\frac{d\varepsilon^3 e_3}{dt/\varepsilon} &= -k_1 |\varepsilon x_1 + \varepsilon w_1(t)|^{\alpha_1} sign(e_1 + w_1(t)) \\
&\quad - \frac{k_2}{\varepsilon^{2\alpha_2}} \left|\varepsilon^2 e_2 - \varepsilon^2 d(t)\right|^{\alpha_2} sign(e_2 - d(t)) \\
&\quad - k_3 \left|\varepsilon^3 x_3 + \varepsilon^3 w_3(t)\right|^{\alpha_3} sign(e_3 + w_3(t)) \\
&\quad - \varepsilon^4 c_\sigma(t)
\end{aligned} \tag{69}$$

Let

$$\begin{aligned}
\tau &= t/\varepsilon; z_i(\tau) = \varepsilon^i e_i(t), \bar{w}_i(\tau) = \varepsilon^i w_i(t), \\
i &= 1, 2, 3; z = [\ z_1 \quad z_2 \quad z_3\ ]^T; \\
\bar{w}_4(\tau) &= \varepsilon^4 c_\sigma(t), \bar{d}(\tau) = \varepsilon^2 d(t)
\end{aligned} \tag{70}$$

we obtain $z = \Xi(\varepsilon) e$. Eq. (69) can be written as

$$\begin{aligned}
\frac{dz_1}{d\tau} &= z_2; \frac{dz_2}{d\tau} = z_3; \\
\frac{dz_3}{d\tau} &= -k_1 |z_1 + \bar{w}_1(\tau)|^{\alpha_1} sign(z_1 + \bar{w}_1(\tau)) \\
&\quad - \frac{k_2}{\varepsilon^{2\alpha_2}} \left|z_2 - \bar{d}(\tau)\right|^{\alpha_2} sign\left(z_2 - \bar{d}(\tau)\right) \\
&\quad - k_3 |z_3 + \bar{w}_3(\tau)|^{\alpha_3} sign(z_3 + \bar{w}_3(\tau)) \\
&\quad - \bar{w}_4(\tau)
\end{aligned} \tag{71}$$

Furthermore, Eq. (71) can be rewritten as

$$\begin{aligned}
\frac{dz_1}{d\tau} &= z_2; \frac{dz_2}{d\tau} = z_3; \\
\frac{dz_3}{d\tau} &= -k_1 |z_1|^{\alpha_1} sign(z_1) - \frac{k_2}{\varepsilon^{2\alpha_2}} |z_2|^{\alpha_2} sign(z_2) \\
&\quad - k_3 |z_3|^{\alpha_3} sign(z_3) \\
&\quad - k_1 \{|z_1 + \bar{w}_1(\tau)|^{\alpha_1} sign(z_1 + \bar{w}_1(\tau)) \\
&\quad - |z_1|^{\alpha_1} sign(z_1)\} \\
&\quad - \frac{k_2}{\varepsilon^{2\alpha_2}} \{\left|z_2 - \bar{d}(\tau)\right|^{\alpha_2} sign\left(z_2 - \bar{d}(\tau)\right) \\
&\quad - |z_2|^{\alpha_2} sign(z_2)\} \\
&\quad - k_3 \{|z_3 + \bar{w}_3(\tau)|^{\alpha_3} sign(z_3 + \bar{w}_3(\tau)) \\
&\quad - |z_3|^{\alpha_3} sign(z_3)\} - \bar{w}_4(\tau)
\end{aligned} \tag{72}$$

Let

$$\begin{aligned}
g_2(\tau, z(\tau)) &= -k_1 \{|z_1 + \bar{w}_1(\tau)|^{\alpha_1} sign(z_1 + \bar{w}_1(\tau)) \\
&\quad - |z_1|^{\alpha_1} sign(z_1)\} \\
&\quad - \frac{k_2}{\varepsilon^{2\alpha_2}} \{\left|z_2 - \bar{d}(\tau)\right|^{\alpha_2} sign\left(z_2 - \bar{d}(\tau)\right) \\
&\quad - |z_2|^{\alpha_2} sign(z_2)\} \\
&\quad - k_3 \{|z_3 + \bar{w}_3(\tau)|^{\alpha_3} sign(z_3 + \bar{w}_3(\tau)) \\
&\quad - |z_3|^{\alpha_3} sign(z_3)\} - \bar{w}_4(\tau)
\end{aligned} \tag{73}$$

Therefore, we obtain

$$\begin{aligned}
\delta &= \sup_{(\tau,z) \in R^4} |g_2(\tau, z(\tau))| \leq 2^{1-\alpha_1} k_1 h_1^{\alpha_1} \varepsilon^{\alpha_1} \\
&\quad + 2^{1-\alpha_3} k_3 h_3^{\alpha_3} \varepsilon^{3\alpha_3} + \varepsilon^4 L_a + 2^{1-\alpha_2} k_2 L_d^{\alpha_2} \\
&\leq \varepsilon^{\rho} \delta_0 + 2^{1-\alpha_2} k_2 L_d^{\alpha_2}
\end{aligned} \tag{74}$$

where $\delta_0 = 2^{1-\alpha_1} k_1 h_1^{\alpha_1} + 2^{1-\alpha_3} k_3 h_3^{\alpha_3} + L_a$, and $\rho = \min_{i \in \{1,3\}} \{\min\{4, i\alpha_i\}\} = \alpha_1$. In fact, when $n = 3$, it is checked that the recursive form of (64) may be rewritten in the non-recursive form

$$\alpha_i = \frac{\alpha_3}{(4 - i) - (3 - i)\alpha_3}, i = 1, 2, 3 \tag{75}$$

Defining the following function

$$g_3(\zeta) = \frac{\zeta \alpha_3}{(4 - \zeta) - (3 - \zeta)\alpha_3}, \zeta \in (0, 4) \tag{76}$$

and taking derivative of $g_3(\zeta)$ with respect to ζ, we obtain

This article has been accepted for publication in a future issue of this journal, but has not been fully edited. Content may change prior to final publication. Citation information: DOI 10.1109/TAES.2017.2668078, IEEE Transactions on Aerospace and Electronic Systems

$$\frac{dg_3(\zeta)}{d\zeta} = \frac{\alpha_3(4-3\alpha_3)}{[(4-\zeta)-(3-\zeta)\alpha_3]^2} > 0 \tag{77}$$

Because $\alpha_3 \in (0,1)$, function $g_3(\zeta)$ is monotone increasing for $\zeta \in (0,4)$. Moreover, the sequence $\{1,2,3\}$ is monotone increasing in open interval $(0,4)$. Therefore,

$$\min_{i\in\{1,3\}} \{i\alpha_i\} = \alpha_1 \tag{78}$$

Furthermore, because $\varepsilon \in (0,1)$ and $\alpha_i \in (0,1)$, $i = 1,2,3$, we obtain

$$\max_{i\in\{1,3\}} \{\varepsilon^{i\alpha_i}\} = \varepsilon^{\rho} = \varepsilon^{\alpha_1} \tag{79}$$

From Proposition 8.1 in [38], Theorem 5.2 in [37] and Eq. (74), for Eq. (72), there exist positive constants μ and $\Gamma(z(0))$, such that, for $\forall \tau \in [\Gamma(z(0)), \infty)$,

$$\|z(\tau)\| \le \mu\delta^{\gamma} \le \mu(\varepsilon^{\alpha_1}\delta_0 + 2^{1-\alpha_2}k_2L_d^{\alpha_2})^{\gamma} \tag{80}$$

where μ is a constant defined in Theorem 5.2 in [37]. Therefore, from coordinate transformation (70), we obtain

$$\| \ \varepsilon e_1 \quad \varepsilon^2 e_2 \quad \varepsilon^3 e_3 \ \| \le \mu(\varepsilon^{\alpha_1}\delta_0 + 2^{1-\alpha_2}k_2L_d^{\alpha_2})^{\gamma} \tag{81}$$

for $\forall t \in [\varepsilon\Gamma(\Xi(\varepsilon)e(0)), \infty)$. Thus, the following inequality holds:

$$|e_i| \le L(\delta_{di})^{\gamma}, i = 1,2,3, \forall t \in [\varepsilon\Gamma(\Xi(\varepsilon)e(0)), \infty) \tag{82}$$

where $L = \mu\delta_0^{\gamma}$; $\delta_{di} = \varepsilon^{\alpha_1 - \frac{i}{\gamma}} + \frac{2^{1-\alpha_2}}{\delta_0}k_2L_d^{\alpha_2}\varepsilon^{-\frac{i}{\gamma}}$, $i = 1,2,3$. If $\varepsilon \in (0,1)$ and $L_d < \left(\frac{1-\varepsilon^{\alpha_1}}{2^{1-\alpha_2}k_2}\delta_0\right)^{\frac{1}{\alpha_2}}$, then

$$0 < \varepsilon^{\alpha_1} + \frac{2^{1-\alpha_2}}{\delta_0}k_2L_d^{\alpha_2} < 1 \tag{83}$$

Furthermore, from Theorem 4.3 in [37], β_c can be chosen to be arbitrarily small. Hence, the requirement that β_c lies on

$$\beta_c \in \left(0, \min\left\{\frac{1}{\frac{4\log\varepsilon}{\log(\varepsilon^{\alpha_1}+\frac{2^{1-\alpha_2}}{\delta_0}k_2L_d^{\alpha_2})}+1}, \frac{1}{2}\right\}\right) \tag{84}$$

is not restrictive. Accordingly, we can obtain

$$\gamma = \frac{1-\beta_c}{\beta_c} > \max\left\{\frac{4\log\varepsilon}{\log(\varepsilon^{\alpha_1}+\frac{2^{1-\alpha_2}}{\delta_0}k_2L_d^{\alpha_2})}, 1\right\} \tag{85}$$

Therefore,

$$\gamma\log(\varepsilon^{\alpha_1} + \frac{2^{1-\alpha_2}}{\delta_0}k_2L_d^{\alpha_2}) < 4\log\varepsilon \tag{86}$$

i.e.,

$$\varepsilon^{\alpha_1} + \frac{2^{1-\alpha_2}}{\delta_0}k_2L_d^{\alpha_2} < \varepsilon^{\frac{4}{\gamma}} \tag{87}$$

From Eq. (85), $\gamma > 4$ holds. Therefore, from $\varepsilon \in (0,1)$, we can obtain $\varepsilon^{\frac{4}{\gamma}} < \varepsilon^{\frac{i}{\gamma}}, i = 1,2,3$. Then

$$\delta_{di} = \varepsilon^{\alpha_1 - \frac{i}{\gamma}} + \frac{2^{1-\alpha_2}}{\delta_0}k_2L_d^{\alpha_2}\varepsilon^{-\frac{i}{\gamma}} < 1 \tag{88}$$

where $i = 1,2,3$. The choice of β_c leads to $\gamma > 1$ in (82) which implies that for $\delta_{di} \in (0,1)$, the ultimate bound (82) on the estimation error is of higher order than the perturbation. Consequently, the presented double-integral observer leads to perform rejection of low-level persistent disturbances.

Ideally, if no noise exist in the measurement signal, i.e, $y_{op} = w_2(t)$ or $L_d = 0$, then (82) can be written as

$$|e_i| \le L\varepsilon^{\alpha_1\gamma - i}, i = 1,2,3, \forall t \in [\varepsilon\Gamma(\Xi(\varepsilon)e(0)), \infty) \tag{89}$$

To make $\alpha_1\gamma - i > 1$, $i = 1,2,3$, from Theorem 5.2 in [37], we let

$$\beta_c \in (0, \min\{\alpha_1/(\alpha_1+4), 1/2\}) = (0, \alpha_1/(\alpha_1+4)) \tag{90}$$

In fact, from Theorem 4.3 in [37], β_c can be chosen to be arbitrarily small. Hence, the requirement that β_c lies on $\beta_c \in (0, \alpha_1/(\alpha_1+4))$ is not restrictive. Accordingly, we can obtain $\alpha_1[(1-\beta_c)/\beta_c] > 4$. Therefore, $\alpha_1\gamma - i > 1$ for $i = 1,2,3$. The choice of β_c leads to $\alpha_1\gamma - i > 1$ in (89) which implies that for $\varepsilon \in (0,1)$, the ultimate bound (89) on the estimation error is of higher order than the perturbation.

For arbitrary $\varepsilon \in (0,1)$, from the Routh-Hurwitz Stability Criterion, polynomial $s^3 + k_3s^2 + \frac{k_2}{\varepsilon^{2\alpha_2}}s + k_1$ is Hurwitz if $k_1 > 0, k_3 > 0, k_2 > \varepsilon^{2\alpha_2}k_1/k_3$. This concludes the proof. ■

Proof of Corollary 1: The Laplace transformations of Eqs. (10) and (4) can be obtained as follows:

$$\begin{aligned} sW_1(s) &= W_2(s) \\ sW_2(s) &= W_3(s) + \Pi(s) \\ sW_3(s) &= c_\sigma(s) \end{aligned} \tag{91}$$

and

$$\begin{aligned} sX_1(s) &= X_2(s) \\ sX_2(s) &= X_3(s) + \Pi(s) \\ \varepsilon^4 sX_3(s) &= -k_1\varepsilon X_1(s) - k_2(X_2(s) - W_2(s)) \\ &\quad -k_3\varepsilon^3 X_3(s) \end{aligned} \tag{92}$$

where $X_i(s)$, $Wi(s)$ and $\Pi(s)$ denote the Laplace transformations of x_i, w_i and $\Pi(t)$, respectively, and s denotes Laplace operator. From Eqs. (91) and (92), we obtain the estimations as follows:

1) x_2 estimates w_2: From Eqs. (91) and (92), it follows that

$$\begin{aligned} X_1(s) &= \frac{1}{s}X_2(s) \\ X_3(s) &= sX_2(s) - sW_2(s) + \frac{1}{s}c_\sigma(s) \\ \varepsilon^4 sX_3(s) &= -k_1\varepsilon X_1(s) - k_2(X_2(s) - W_2(s)) \\ &\quad -k_3\varepsilon^3 X_3(s) \end{aligned} \tag{93}$$

Therefore, Eq. (93) can be written as

This article has been accepted for publication in a future issue of this journal, but has not been fully edited. Content may change prior to final publication. Citation information: DOI 10.1109/TAES.2017.2668078, IEEE Transactions on Aerospace and Electronic Systems

$$\begin{aligned}&\varepsilon^4 s\{sX_2(s)-sW_2(s)+\frac{1}{s}c_\sigma(s)\}\\ =\;&-k_1\varepsilon\frac{1}{s}X_2(s)-k_2\left(X_2(s)-W_2(s)\right)\\&-k_3\varepsilon^3\{sX_2(s)-sW_2(s)+\frac{1}{s}c_\sigma(s)\}\end{aligned}\quad(94)$$

Then, it follows that

$$\begin{aligned}X_2(s) &= \frac{\varepsilon^4 s^3+k_3\varepsilon^3 s^2+k_2 s}{\varepsilon^4 s^3+k_3\varepsilon^3 s^2+k_2 s+k_1\varepsilon}W_2(s)\\&-\frac{\varepsilon^4 s+k_3\varepsilon^3}{\varepsilon^4 s^3+k_3\varepsilon^3 s^2+k_2 s+k_1\varepsilon}c_\sigma(s)\end{aligned}\quad(95)$$

Therefore,

$$\lim_{\varepsilon\to 0}\frac{X_2(s)}{W_2(s)}=1\quad(96)$$

2) x_1 estimates w_1: From Eqs. (91) and (92), we obtain

$$\begin{aligned}W_2(s) &= sW_1(s)\\W_3(s) &= \frac{1}{s}c_\sigma(s)\\\Pi(s) &= s^2W_1(s)-\frac{1}{s}c_\sigma(s)\end{aligned}\quad(97)$$

and

$$\begin{aligned}X_2(s) &= sX_1(s)\\X_3(s) &= s^2X_1(s)-s^2W_1(s)+\frac{1}{s}c_\sigma(s)\\\varepsilon^4 sX_3(s) &= -k_1\varepsilon X_1(s)-k_2\left(X_2(s)-W_2(s)\right)\\&\quad-k_3\varepsilon^3X_3(s)\end{aligned}\quad(98)$$

Therefore, Eqs. (97) and (98) can be written as

$$\begin{aligned}&\varepsilon^4 s\{s^2X_1(s)-s^2W_1(s)+\frac{1}{s}c_\sigma(s)\}\\ =\;&-k_1\varepsilon X_1(s)-k_2\left(sX_1(s)-sW_1(s)\right)\\&-k_3\varepsilon^3\{s^2X_1(s)-s^2W_1(s)+\frac{1}{s}c_\sigma(s)\}\end{aligned}\quad(99)$$

Then, it follows that

$$\begin{aligned}X_1(s) &= \frac{\varepsilon^4 s^3+k_3\varepsilon^3 s^2+k_2 s}{\varepsilon^4 s^3+k_3\varepsilon^3 s^2+k_2 s+k_1\varepsilon}W_1(s)\\&-\frac{\varepsilon^4+k_3\varepsilon^3\frac{1}{s}}{\varepsilon^4 s^3+k_3\varepsilon^3 s^2+k_2 s+k_1\varepsilon}c_\sigma(s)\end{aligned}\quad(100)$$

Therefore,

$$\lim_{\varepsilon\to 0}\frac{X_1(s)}{W_1(s)}=1\quad(101)$$

3) x_3 estimates w_3: From Eqs. (91) and (92), we obtain

$$\begin{aligned}W_2(s) &= \frac{1}{s}W_3(s)+\frac{1}{s}\Pi(s)\\X_1(s) &= \frac{1}{s}X_2(s)\\X_2(s) &= \frac{1}{s}X_3(s)+\frac{1}{s}\Pi(s)\\\varepsilon^4 sX_3(s) &= -k_1\varepsilon X_1(s)-k_2\left(X_2(s)-W_2(s)\right)\\&\quad-k_3\varepsilon^3X_3(s)\end{aligned}\quad(102)$$

Therefore, Eq. (102) can be written as

$$\begin{aligned}\varepsilon^4 s^3X_3(s) &= -k_1\varepsilon X_3(s)-k_1\varepsilon\Pi(s)-k_2sX_3(s)\\&\quad-k_2s\Pi(s)+k_2sW_3(s)+k_2s\Pi(s)\\&\quad-k_3\varepsilon^3s^2X_3(s)\end{aligned}\quad(103)$$

Then, it follows that

$$\begin{aligned}X_3(s) &= \frac{k_2 s}{\varepsilon^4 s^3+k_3\varepsilon^3 s^2+k_2 s+k_1\varepsilon}W_3(s)\\&-\frac{k_1\varepsilon}{\varepsilon^4 s^3+k_3\varepsilon^3 s^2+k_2 s+k_1\varepsilon}\Pi(s)\end{aligned}\quad(104)$$

Therefore,

$$\lim_{\varepsilon\to 0}\frac{X_3(s)}{W_3(s)}=1\quad(105)$$

It means that x_i approximates w_i for $i=1,2,3$. Furthermore, the denominator of Eq. (95) (also in Eqs. (100) and (104)) is required to be Hurwitz, i.e., $s^3+\frac{k_3}{\varepsilon}s^2+\frac{k_2/\varepsilon^2}{\varepsilon^2}s+\frac{k_1}{\varepsilon^3}$ is Hurwitz. It is equivalent that $s^3+k_3s^2+\frac{k_2}{\varepsilon^2}s+k_1$ should be Hurwitz. For arbitrary $\varepsilon\in(0,1)$, from the Routh-Hurwitz Stability Criterion, this polynomial is Hurwitz if $k_1>0$, $k_3>0$, $k_2>\varepsilon^2k_1/k_3$. This concludes the proof. ■

REFERENCES

[1] Whittenbury, J. R. "Configuration design development of the navy UCAS-D X-47B," AIAA Centennial of Naval Aviation Forum "100 Years of Achievement and Progress," Virginia Beach, VA, Sep. 21-22, 2011.

[2] MacKunis, W., Subramanian, S., Mehta,S., Ton, C., Curtis, J. W., and Reyhanoglu, M. "Robust nonlinear aircraft tracking control using synthetic jet actuators," IEEE Conference on Decision and Control, Firenze, Dec. 10-13, 2013.

[3] Rathay, N., Boucher, M., Amitay, M., and Whalen, E. "Parametric study of synthetic-jet-based control for performance enhancement of a vertical tail," AIAA Journal, 52, 11 (2014), 2440-2454.

[4] Scherer, P. O. J. Computational Physics. Berlin, Germany: Springer-Verlag, 2008.

[5] Tseng, C. C., and Lee,S. L. "Digital IIR integrator design using recursive Romberg integration rule and fractional sample delay," Signal Process., 88, 9 (2008), 2222-2233.

[6] Ngo, N. Q. "A new approach for the design of wideband digital integrator and differentiator," IEEE Trans. Circuits and Syst. II, Exp. Briefs, 53, 9 (2008), 936-940.

[7] Al-Alaoui, M. A. "Low-frequency differentiators and integrators for biomedical and seismic signals," IEEE Trans. Circuits Sys. I: Fundam. Theory Appl., 48, 8 (2001), 1006-1011.

[8] Charef, A., Sun, H. H., Tsao, Y. Y., and Onaral, B. "Fractal system as represented by singularity function," IEEE Trans. Autom. Control, 37, 9 (1992), 1465-1470.

[9] Atassi, A. N., and Khalil, H. K. "Separation results for the stabilization of nonlinear systems using different high-gain observer designs," Syst. Control Lett., 39, 3 (2000), 183-191.

[10] Levant, A. "High-order sliding modes, differentiation and output-feedback control," Int. J. of Control, 76, 9/10 (2003), 924-941.

[11] Wang, X., Chen, Z., and Yang, G. "Finite-time-convergent differentiator based on singular perturbation technique," IEEE Trans. Autom. Control, 52, 9 (2007), 1731-1737.

[12] Wang, X., and Shirinzadeh, B. "High-order nonlinear differentiator and application to aircraft control," Mech. Sys. Signal Process., 46, 2 (2014), 227-252.

[13] Auger, F., Hilairet, M., Guerrero, J. M., and Monmasson, E. "Industrial applications of the Kalman filter: A Review," IEEE Trans. Ind. Electron., 60, 12 (2013), 5458-5471.

[14] Idkhajine, L., Monmasson, E., and Maalouf, A. "Fully FPGA-based sensorless control for synchronous AC drive Using an Extended Kalman filter," IEEE Trans. Ind. Electron., 59, 10 (2012), 3908-3918.

[15] Wang, X., Shirinzadeh, B., and Ang, M.H. "Nonlinear double-integral observer and application to quadrotor aircraft," IEEE Trans. Ind. Electron., 62, 2 (2015), 1189-1200.

[16] Wang, X., and Shirinzadeh, B. "Nonlinear multiple integrator and application to aircraft navigation," IEEE Trans. Aerosp. Electron. Syst., 50, 1 (2014), 607-622.

[17] Wang, X., and Shirinzadeh, B. "Nonlinear continuous integral-derivative observer," Nonlinear Dyn., 77, 3 (2014), 793-806.

[18] Hahn, J. O., Rajamani, R., You, S. H., and Lee, K. I. "Real-time identification of road-bank angle using differential GPS," IEEE Trans. Control Syst. Technol., 12, 4 (2004), 589-599.

[19] Abdel-Hafez, M.F. "Detection of bias in GPS satellites' measurements: A probability ratio test formulation," IEEE Trans. Control Syst. Technol., 22, 3 (2014), 1166-1173.

[20] Yu, M. J. "INS/GPS integration system using adaptive filter for estimating measurement noise variance," IEEE Trans. Aerosp. Electron. Syst., 48, 2 (2012), 1786-1792.

[21] Cho, S. "IM-filter for INS/GPS-integrated navigation system containing low-cost gyros," IEEE Trans. Aerosp. Electron. Syst., 50, 4 (2014), 2619-2629.

[22] Sadi, F., and Klukas, R. "New jump trajectory determination method using low-cost MEMS sensor fusion and augmented observations for GPS/INS integration," GPS Solutions, 17, 2 (2013), 139-152.

[23] Kendoul, F., Lara, D., Fantoni-Coichot, I., and Lozano, R. "Real-time nonlinear embedded control for an autonomous quadrotor helicopter," Journal of Guidance, Control, and Dynamics, 30, 4 (2007), 1049–1061.

[24] Salazar-Cruz, S., Escareno, J., Lara, J., and Lozano, R. "Embedded control system for a four-rotor UAV," International Journal of Adaptive Control and Signal Processing, 21, 2/3 (2007), 189–204.

[25] Hoffmann, G., Huang, H., Waslander, S., and Tomlin, C. "Quadrotor helicopter flight dynamics and control: Theory and experiment," AIAA Guidance, Navigation and Control Conference and Exhibit, Hiltion Head, South Carolina, Aug. 20-23, 2007, pp. 1670–1689.

[26] Grzonka, S., Grisetti, G., and Burgard, W. "Towards a navigation system for autonomous indoor flying," IEEE Int. Conf. on Robotics and Automation, Kobe, May 12-17, 2009, pp. 2878–2883.

[27] Hamela, T., and Mahony, R. "Image based visual servo control for a class of aerial robotic system," Automatica, 43, 11 (2007), 1976-1983.

[28] Guenard, N., Hamel, T., and Mahony, R. "A practical visual servo control for an unmanned aerial vehicle," IEEE Transactions on Robotics, 24, 2 (2008), 331–340.

[29] Kendoul, F., Fantoni, I., and Nonami, K. "Optic flow-based vision system for autonomous 3d localization and control of small aerial vehicles," Robotics and Autonomous Systems, 57, 6/7 (2009), 591–602.

[30] Valenti, M., Bethke, B., Fiore, G., How, J. P., and Feron, E. "Indoor Multi-Vehicle Flight Testbed for Fault Detection, Isolation, and Recovery," AIAA Guidance, Navigation, and Control Conference (GNC), Keystone, CO, (AIAA-2006-6200), 2006, 1–18.

[31] How, J. P., McGrew, J., Frank, A., and Hines, G. "Autonomous aircraft flight control for constrained environments," IEEE International Conference on Robotics and Automation, ICRA 2008, Pasadena, CA, May 19-23, 2008, pp. 2213–2214.

[32] Achtelik, M., Bachrach, A., He, R., Prentice, S., and Roy, N. "Stereo vision and laser odometry for autonomous helicopters in GPS-denied indoor environments," Proc. SPIE, Apr., 7332 (2009), 733219-1–733219-10.

[33] Hwang, C. L. "Hybrid neural network under-actuated sliding-mode control for trajectory tracking of quad-rotor unmanned aerial vehicle," The 2012 International Joint Conference on Neural Networks (IJCNN), Brisbane, QLD, Jun. 10-15, 2012, pp. 1–8.

[34] Yeh, F. K. "Attitude controller design of mini-unmanned aerial vehicles using fuzzy sliding-mode control degraded by white noise interference," IET Control Theory & Applications, 6, 9 (2012), 1205–1212.

[35] Park, J., and Sandberg, I. W. "Universal approximation using radial-basis-function networks," Neural Comput. 3 (1991), 246–257.

[36] Wang, L. X. "Fuzzy systems are universal approximations," In: Proceedings of the IEEE International Conference on Fuzzy Systems, San Diego, Mar. 8–12, 1992, pp. 1163–1170.

[37] Bhat S. P., and Bernstein, D. S. "Finite-time stability of continuous autonomous systems," Siam J. Control Optim., 38, 3 (2000), 751-766.

[38] Bhat S. P., and Bernstein, D. S. "Geometric homogeneity with applications to finite-time stability," Mathematics of Control, Signals, and Systems, 17, 2 (2005), 101-127.

[39] Lee J. I., and Ha, I. J. "A novel approach to control of nonminimum-phase nonlinear systems," IEEE Trans. Autom. Control, 47, 9 (2002), 1480-1486.

[40] Kahlil, H. "Nonlinear systems," 3nd ed. Englewood Cliffs, New Jerse: Prentice-Hall, 2002.

[41] Wang, X., and Shirinzadeh, B. "Nonlinear augmented observer design and application to quadrotor aircraft," Nonlinear Dynamics, 80, 3 (2015), 1463-1481.

[42] Slotine, J. J. E., and Li, W. "Applied nonlinear control," Englewood Cliffs, NJ: Prentice-Hall,1991.

[43] Sanchez, A. M., Prieto, R., Laso, M., and Riesgo, T. "A piezoelectric minirheometer for measuring the viscosity of polymer microsamples," IEEE Trans. Ind. Electron., 55, 1 (2008), 427-436.

[44] Katagiri, Y., Takesue, H., and Hashimoto, E. "Wavelength-scanning optical bandpass filters based on optomechatronics for optical-frequency sweepers," IEEE Trans. Ind. Electron., 52, 4 (2005), 992-1004.

[45] Boelens, O. J. "CFD analysis of the flow around the X-31 aircraft at high angle of attack," Aerosp. Sci. Technol., 20, 1 (2012), 38-51.

[46] Fan, P., Wang, X., and Cai, K. "Design and control of a tri-rotor aircraft," Control and Automation (ICCA), 2010 8th IEEE International Conference on, Xiamen, June 9-11, 2010, pp. 1972-1977.

Xinhua Wang received his Ph.D in control theory and control engineering from Nankai University, China, in 2004.
He was, respectively, a research fellow at the Dept. of Electrical and Computer Engineering, National University of Singapore, Singapore; a research officer at the Dept. of Mechanical and Aerospace Engineering, Monash University, Australia; a visiting scholar at the Dept. of Mechanical and Aerospace Engineering, Hong Kong University of Science and Technology, Hong Kong. He is currently an assistant professor at the Dept. of Electrical and Electronic Engineering, University of Nottingham, United Kingdom. His research interests include signal estimation and processing, new conceptual aircraft design and control, VTOL aircraft control, 4WS and 4WD vehicle design and control, navigation and guidance.

Lilong Cai received his B.Eng. degree in the Department of Precision Instrumentation Engineering from Tianjin University, Tianjin, China, in 1982 and PhD degree in Department of Mechanical Engineering, from University of Toronto, Canada. From 1990 to 1993, he was an Assistant Professor at the Department of Mechanical Engineering, Columbia University, New York City, USA. He has been the Hong Kong University of Science and Technology (HKUST) since 1993. Currently, he is Professor in the Department of Mechanical and Aerospace Engineering, HKUST. He has published 59 referred international journal papers and 75 papers at international conferences proceedings. He holds three US patents. His research interests are in the control of nonlinear system, robotics, measurement and mechatronics.